Taylor & Francis
Taylor & Francis Group

RESEARCH PAPER

A chemical genomics-aggrephagy integrated method studying functional analysis of autophagy inducers

Tetsushi Kataura[a,b,†], Etsu Tashiro[a,††], Shota Nishikawa[a], Kensuke Shibahara[a], Yoshihito Muraoka[a], Masahiro Miura[a], Shun Sakai[a], Naohiro Katoh[a], Misato Totsuka[a], Masafumi Onodera[c], Kazuo Shin-Ya [d,e,f], Kengo Miyamoto[g], Yukiko Sasazawa[a,g], Nobutaka Hattori[g], Shinji Saiki[g], and Masaya Imoto [a,†,†††]

aDepartment of Biosciences and Informatics, Keio University, Kanagawa, Japan; bResearch Fellow of the Japan Society for the Promotion of Science (JSPS), Tokyo, Japan; cDivision of Immunology, National Center for Child Health and Development, Tokyo, Japan; dNational Institute of Advanced Industrial Science and Technology, Tokyo, Japan; eBiotechnology Research Centre, The University of Tokyo, Tokyo, Japan; fCollaborative Research Institute for Innovative Microbiology, The University of Tokyo, Tokyo, Japan; gDepartment of Neurology, Juntendo University School of Medicine, Tokyo, Japan

ABSTRACT

Macroautophagy/autophagy plays a critical role in the pathogenesis of various human diseases including neurodegenerative disorders such as Parkinson disease (PD) and Huntington disease (HD). Chemical autophagy inducers are expected to serve as disease-modifying agents by eliminating cytotoxic/damaged proteins. Although many autophagy inducers have been identified, their precise molecular mechanisms are not fully understood because of the complicated crosstalk among signaling pathways. To address this issue, we performed several chemical genomic analyses enabling us to comprehend the dominancy among the autophagy-associated pathways followed by an aggresome-clearance assay. In a first step, more than 400 target-established small molecules were assessed for their ability to activate autophagic flux in neuronal PC12D cells, and we identified 39 compounds as autophagy inducers. We then profiled the autophagy inducers by testing their effect on the induction of autophagy by 200 well-established signal transduction modulators. Our principal component analysis (PCA) and clustering analysis using a dataset of "autophagy profiles" revealed that two Food and Drug Administration (FDA)-approved drugs, memantine and clemastine, activate endoplasmic reticulum (ER) stress responses, which could lead to autophagy induction. We also confirmed that SMK-17, a recently identified autophagy inducer, induced autophagy via the PRKC/PKC-TFEB pathway, as had been predicted from PCA. Finally, we showed that almost all of the autophagy inducers tested in this present work significantly enhanced the clearance of the protein aggregates observed in cellular models of PD and HD. These results, with the combined approach, suggested that autophagy-activating small molecules may improve proteinopathies by eliminating nonfunctional protein aggregates.

Abbreviations: ADK: adenosine kinase; AMPK: AMP-activated protein kinase; ATF4: activating transcription factor 4; BECN1: beclin-1; DDIT3/CHOP: DNA damage inducible transcript 3; EIF2AK3/PERK: eukaryotic translation initiation factor 2 alpha kinase 3; EIF2S1/eIF2α: eukaryotic translation initiation factor 2 subunit alpha; ER: endoplasmic reticulum; ERN1/IRE1α: endoplasmic reticulum to nucleus signaling 1; FDA: Food and Drug Administration; GSH: glutathione; HD: Huntington disease; HSPA5/GRP78: heat shock protein family A (Hsp70) member 5; HTT: huntingtin; JAK: Janus kinase; MAP1LC3B/LC3: microtubule associated protein 1 light chain 3 beta; MAP2K/MEK: mitogen-activated protein kinase kinase; MAP3K8/Tpl2: mitogen-activated protein kinase kinase kinase 8; MAPK: mitogen-activated protein kinase; MPP⁺: 1-methyl-4-phenylpyridinium; MTOR: mechanistic target of rapamycin kinase; MTORC: MTOR complex; NAC: N-acetylcysteine; NGF: nerve growth factor 2; NMDA: N-methyl-D-aspartate; PCA: principal component analysis; PD: Parkinson disease; PDA: pancreatic ductal adenocarcinoma; PIK3C3: phosphatidylinositol 3-kinase catalytic subunit type 3; PMA: phorbol 12-myristate 13-acetate; PRKC/PKC: protein kinase C; ROCK: Rho-associated coiled-coil protein kinase; RR: ribonucleotide reductase; SIGMAR1: sigma non-opioid intracellular receptor 1; SQSTM1/p62: sequestosome 1; STK11/LKB1: serine/threonine kinase 11; TFEB: Transcription factor EB; TGFB/TGF-β: Transforming growth factor beta; ULK1: unc-51 like autophagy activating kinase 1; XBP1: X-box binding protein 1.

CONTACT Masaya Imoto ✉ imoto.a6@keio.jp Division for Development of Autophagy Modulating Drugs, Juntendo University Graduate School of Medicine, 2-1-1, Hongo, Bunkyo, Tokyo, 113-8421 Japan
†Present address: Department of Neurology, Juntendo University School of Medicine, Tokyo, Japan
††Present address: Laboratory of Biochemistry, Showa Pharmaceutical University, Tokyo, Japan
†††Present address: Division for Development of Autophagy Modulating Drugs, Juntendo University Graduate School of Medicine, Tokyo, Japan

Supplemental data for this article can be accessed here.

Introduction

Macroautophagy/autophagy, an intracellular degradation system for recycling damaged organelles and removing aggregated proteins via lysosomes, is an essential process that maintains cellular homeostasis [1]. Given that impairment of autophagy has been implicated in various diseases such as cancer, infections, and neurodegenerative disease [2], stimulating autophagy by small-molecule chemical compounds has been proposed as a therapeutic intervention [3]. While many autophagy inducers have been identified so far, their mechanisms of autophagy induction remain (in some cases) poorly understood, probably because of the highly diversified and complicated crosstalk among autophagy signaling pathways, which include both MTOR (mechanistic target of rapamycin kinase)-dependent and -independent processes [4].

MTOR inhibitors such as rapamycin and torin1 are the best-understood autophagy inducers. The MTOR complex 1 (MTORC1) negatively regulates autophagy by phosphorylating ULK1 (unc-51 like autophagy activating kinase 1) required for autophagosome formation [5] and TFEB (transcription factor EB) known as a master regulator of autophagy/lysosome gene expression [6]. Inhibitors that act upstream of MTOR including AKT (AKT serine/threonine kinase) and TP53/p53 (tumor protein p53); activators that act downstream of MTOR are expected to be inducers of autophagy. Conversely, small molecules that modulate the inositol, Ca^{2+}-CAPN/calpain, cAMP (cyclic adenosine monophosphate), or BECN1 (beclin-1) signaling pathways activate autophagy in an MTOR-independent manner. In addition, activators of TFEB or other transcription factors that are involved in the expression of autophagy genes, such as those encoding the forkhead-box proteins FOXO1 and FOXO3, also are capable of inducing autophagy [7]. Inducers of endoplasmic reticulum (ER) stress also have been implicated in the activation of autophagy through the ER stress response, including effects mediated primarily via ERN1/IRE1α (endoplasmic reticulum to nucleus signaling 1) and EIF2AK3/PERK (eukaryotic translation initiation factor 2 alpha kinase 3) signaling [8].

Thus, autophagy activation by small molecules can be achieved via various pathways, which complicates the analysis of their mechanisms of action. To address this issue, we performed chemical genomic analyses to classify autophagy inducers and facilitate characterization of the autophagy induction mechanism. Magi *et al.* previously demonstrated that cell migration can be controlled by diverse signaling pathways [9]; in that work, the authors used chemical signal transduction modulators as probes to inhibit target protein activity, rather than employing gene silencing. That approach is easily applicable in autophagy research because the strategy only requires adding signal modulators into cell culture medium with autophagy inducers at any desired time point.

In the present study, we firstly conducted a chemical screen and identified 39 compounds as autophagy inducers in neuronal PC12D cells. We then examined the autophagy profile of each of 26 autophagy inducers by chemical genomics. Multiple distinct autophagy profiles were observed.

These were subjected to principal component analysis (PCA) and clustering analysis to infer the mechanism of action of chemical compounds that induce autophagy by unknown mechanisms. Based on our clustering analysis, we identified the mechanism underlying autophagy activation induced by two Food and Drug Administration (FDA)-approved drugs, memantine and clemastine. These two drugs were already reported to induce autophagy [10,11]; however, whose autophagy induction mechanism previously was not understood. In addition, we used our PCA to identify SMK-17, a recently identified MAP2 K/MEK (mitogen-activated protein kinase kinase 1 and 2) inhibitor, as a novel autophagy inducer, and further evaluated this compound's mechanism of autophagy activation. Through these studies, we demonstrated that a chemical genomic approach might be useful for inferring the mode of action of chemical autophagy inducers. Finally, we examined the effect of 26 autophagy inducers on protein aggregation (i.e. the clearance of aggresomes), a hallmark of neurodegenerative disorders [12], using a cellular model of Parkinson disease (PD), demonstrating a contrast to the effects of antioxidants. We showed the superiority of autophagy inducers in removing cytotoxic protein aggregates, which are commonly observed in neurodegenerative disorders including PD and Huntington disease (HD).

Results

Screening of autophagy inducers using a GFP-LC3-RFP autophagy probe in neuronal PC12D cells

Autophagy flux can be evaluated simply by measuring GFP: RFP signal intensity ratio, using a GFP-LC3-RFP probe that produces equal amounts of GFP-LC3 as the autophagy marker (by degradation during the progression of autophagy) and RFP as an internal expression control [13]. We first generated PC12D stably expressing this probe by high-titer retroviral transduction followed by fluorescence-activated cell sorting (FACS) to obtain comparably fluorescent cells (Figure 1A). To validate the utility of the transduced cells as reporters of autophagy, we confirmed that (a) exposure of the cell to the known autophagy inducers rapamycin and torin1 yielded a decreased GFP:RFP ratio and (b) exposure to the known autophagy inhibitor bafilomycin A_1 yielded an increased GFP:RFP ratio (Figure 1B,C). We then screened ~ 400 compounds, primarily from SCADS inhibitor kits (I–IV) consisting of target-identified small molecules, to identify autophagy inducers (Figure 1D,E). Following reevaluation of the top 50 compounds recovered in the 1st screen, we identified 39 compounds that significantly induced autophagy in neuronal PC12D cells (Figure 1F, Table 1 and S1). While 38 of these 39 compounds previously have been reported as autophagy inducers, one (SMK-17) appears to constitute a novel autophagy inducer. Among the 39 autophagy inducers, we selected 26 compounds as non-cytotoxic autophagy inducers (above 80% cell viability, **Fig. S1**) for further investigation.
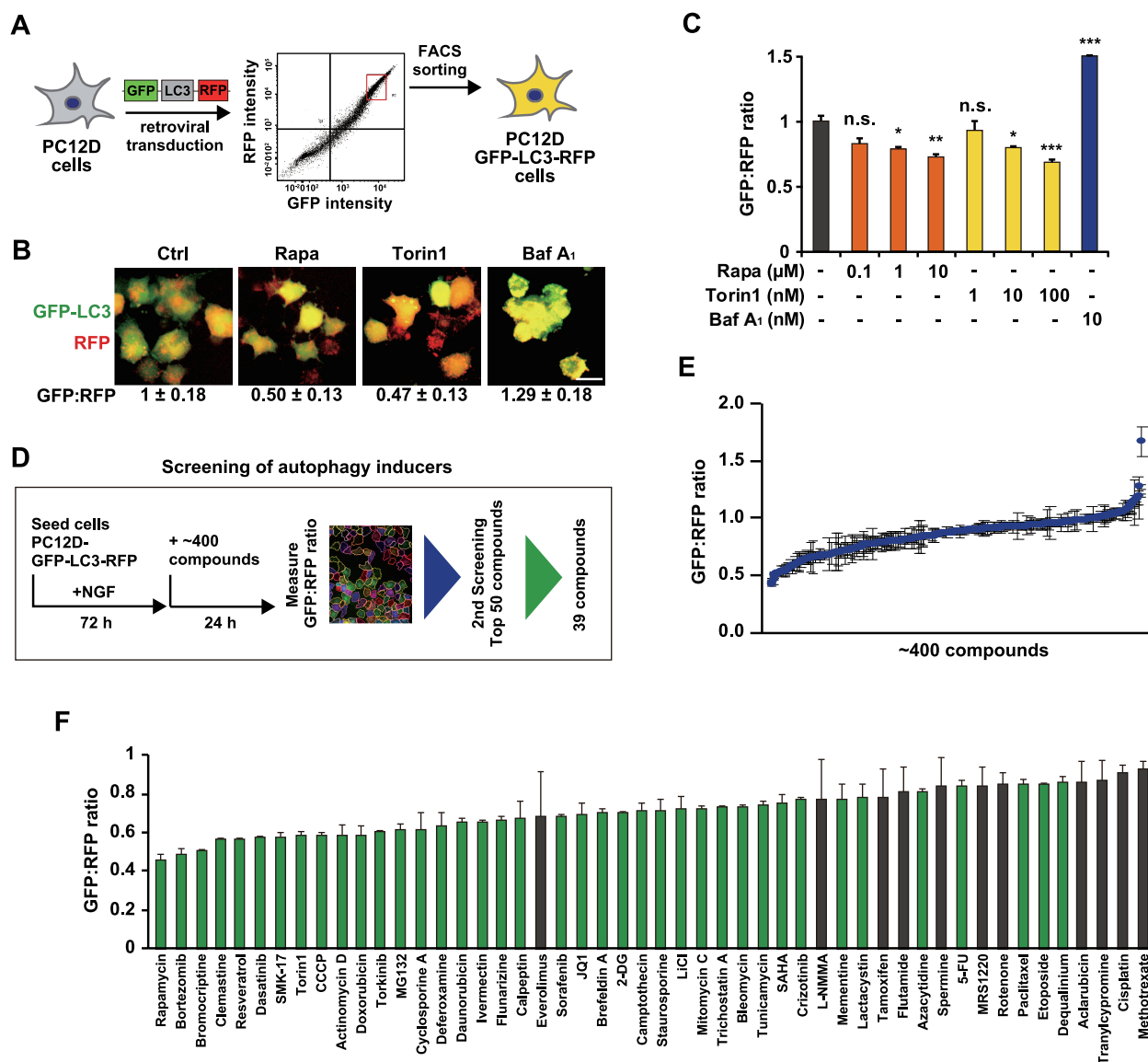
Figure 1. Screening of autophagy inducers in neuronal PC12D cells using GFP-LC3-RFP autophagy flux probe. (A) Schematic illustration of establishment of PC12D cells stably expressing GFP-LC3-RFP autophagy flux probe. (B) PC12D cells expressing GFP-LC3-RFP were treated with 10 μM rapamycin (Rapa), 100 nM torin1, or 10 nM bafilomycin A_1 (Baf A_1) for 24 h. Scale bar: 20 μm. (C) PC12D cells expressing GFP-LC3-RFP were treated with the indicated concentrations of rapamycin, torin1, or bafilomycin A_1 for 24 h. The GFP:RFP fluorescence intensity ratio was measured using a high-content imager. (D) Schematic illustration of the chemical screen. (E) Scatter plot of the GFP:RFP ratio of each compound in the screen. (F) Bar graph showing the GFP:RFP ratios of the top 50 compounds. Green bars indicate compounds that significantly induced autophagy ($p < 0.05$, two-tailed Student's t test compared to control). Data are shown as mean ± SD (n = 3). n.s., non-significant, *$p < 0.05$, **$p < 0.01$, ***$p < 0.001$ (two-tailed one-way ANOVA with post hoc Dunnett's test).

Chemical genomic analyses of autophagy induction patterns associated with small molecules

We used a chemical genomic approach to classify these autophagy inducers based on their modulation of the autophagy induction patterns associated with various known chemical inhibitors. For this purpose, we firstly examined how pre-treatment with 200 well-established signal transduction modulators inhibited the induction of autophagy by 26 autophagy inducers. The autophagy profile associated with each autophagy inducer was obtained by setting the value of the GFP:RFP ratio in untreated cells and single autophagy inducer-treated cells as 1 and 0, respectively (Figure 2A). Highly reproducible datasets from 2 independent experiments were averaged and subjected to PCA and clustering analysis (Figure 2B and Table

S2). On the PC1-PC2 plane, autophagy inducers appeared to group based on their mode of action, given that MTOR inhibitors (rapamycin and torin1), ER stress inducers (2-deoxyglucose and tunicamycin), epigenetic modulators (azacytidine, SAHA, and trichostatin A), and proteasome inhibitors (bortezomib and MG132) yielded closely colocalizing patterns by class (Figure 2C). Epigenetic modulators as well as proteasome inhibitors also were distinctly positioned on the PC3-PC4 plane (Figure 2D). A loading plot showed that some portions of the patterns associated with signaling via cell cycle kinases (AURK [aurora kinase], ATM [ATM serine/threonine kinase] and CDK [cyclin-dependent kinase]), HSP90 (heat shock protein 90), and HIF (hypoxia inducible factor) were coordinated on the PC2 plane, while the patterns associated with a number of signal transduction modulators

Table 1. Autophagy inducers used in this study.

Compound	Concentration	Target	Reference
2-Deoxyglucose (2-DG)	10 mM	Glycolysis	[14]
Azacytidine	10 μM	DNA methyltransferase	[15]
Bortezomib	100 nM	Proteasome	[16]
Brefeldin A	500 nM	COP-I complex	[17]
Bromocriptine	10 μM	Dopamine receptor agonist	[18]
Calpeptin	50 μM	CAPN/calpain	[4]
Clemastine	5 μM	Histamine H1 antagonist	[58]
Crizotinib	5 μM	Tyrosine kinase	[19]
Cyclosporine A	5 μM	Immunosuppressant	[20]
Dasatinib	10 μM	Tyrosine kinase	[21]
Deferoxamine (DFO)	100 μM	Iron chelator	[22]
Flunarizine	20 μM	Calcium antagonist	[62]
Ivermectin	10 μM	Anti-parasite medication	[23]
JQ1	1 μM	BRD4 (bromodomain containing 4)	[33]
LiCl	50 mM	Glycogen synthase kinase 3	[24]
Memantine	100 μM	NMDA receptor antagonist	[10]
MG132	5 μM	Proteasome	[25]
Rapamycin	10 μM	MTORC1	[26]
Resveratrol	100 μM	Polyphenol, SIRT1 activator	[27]
SAHA	3 μM	Histone deacetylase	[28]
SMK-17	10 μM	MAP2 K/MEK 1 and 2	[66]
Sorafenib	2 μM	Protein kinase	[29]
Staurosporine	10 nM	Protein kinase	[30]
Torin1	100 nM	MTORC1, 2	[31]
Trichostatin A	1 μM	Histone deacetylase	[32]
Tunicamycin	2 μM	N-linked glycosylation (ER stress)	[54]

were coordinated on the PC1 plane (Figure 2E). V-type ATPase, PRKC/PKC (protein kinase C), BIRC5/Survivin, and AKT (AKT serine/threonine kinase) inhibitors affected parameters on both the PC1 and PC2 planes (Figure 2E). Parameters on the PC3 and PC4 planes were negatively coordinated by FGFR (fibroblast growth factor receptor), JAK (Janus kinase), SYK (spleen associated tyrosine kinase), NTRK1/TrkA (neurotrophic receptor tyrosine kinase 1) signaling and PIK3CA/PI3K (phosphatidylinositol-4,5-bisphosphate 3-kinase catalytic subunit alpha), TGFB/TGF-β (transforming growth factor beta)-ROCK (Rho-associated coiled-coil protein kinase) signaling, respectively, while ADK (adenosine kinase), RR (ribonucleotide reductase), and MAP3K8/Tpl2 (mitogen-activated protein kinase kinase kinase 8) signaling positively coordinated along the PC4 axis (Figure 2F). Next, we performed a clustering analysis using all of the obtained inhibitory data. As shown in Figure 3A, autophagy inducers classified into approximately 6 distinct groups, including epigenetic modulators (Cluster 1), ER stress inducers (Cluster 2), and proteasome inhibitors (Cluster 6). JQ1 sorted separately from these clusters, possibly reflecting the observation that autophagy induced by JQ1 was not inhibited by almost any of the signal transduction modulators. Given that JQ1 is an inhibitor of BRD4 (bromodomain containing 4), a transcriptional repressor of autophagy/lysosomal genes, we inferred that JQ1 directly induces autophagy in a signal transduction-independent manner [33]. In contrast, autophagy induction by cyclosporine A was inhibited by multiple signal transduction modulators, presumably reflecting the multiple activities of cyclosporine A [34] and explaining the distinct autophagy induction profile associated with this molecule. Among the signal transduction modulators, EHMT2/G9a (euchromatic histone lysine methyltransferase 2),

HSP90 (heat shock protein 90), HIF (hypoxia inducible factor), EIF2AK2/PKR (eukaryotic translation initiation factor 2 alpha kinase 2) and several cell cycle kinase inhibitors showed global inhibition of autophagy (Figure 3B). In line with the results of PCA, modulators of signaling by JAK, STAT (signal transducer and activator of transcription); TGFB, EP300 (E1A binding protein p300), ROCK; and RR, ADK, MAP3K8 selectively inhibited the autophagy induced by compounds within (respectively) Clusters 6, 5, and 1 (Figure 3C). Although specific signaling pathways differing between Clusters 2, 3, and 4 were not observed, similarities of the patterns of the autophagy profiles among these clusters were inferred to be indicative of some shared mechanisms of autophagy induction.

Memantine and clemastine induce ER stress

We observed that memantine, clemastine, and flunarizine, three clinically used drugs, were classified into Cluster 2 with tunicamycin and 2-deoxyglucose, which are known inducers of ER stress. This result raised the possibility that these three clinically used drugs also are inducers of ER stress. As shown in Figure 4A, both the expression levels of DDIT3/CHOP (DNA damage inducible transcript 3) and the phosphorylation levels of EIF2S1/eIF2α (eukaryotic translation initiation factor 2 subunit alpha) were increased by treatment with memantine, clemastine, and flunarizine, as was seen for tunicamycin and 2-deoxyglucose. The expression levels of DDIT3 and the phosphorylation levels of EIF2S1 were increased by the phosphorylation of EIF2AK3, a known sensor of ER stress, and the phosphorylation of EIF2AK3 (as judged by the mobility shift of EIF2AK3 on SDS-PAGE [35–37]) was observed following treatment with memantine and clemastine, though not with flunarizine (Figure 4B). In addition, increased levels of HSPA5/GRP78 (heat shock protein family A [Hsp70] member 5) expression and accumulation of the mRNA encoding spliced *Xbp1* (X-box binding protein 1), which were seen in tunicamycin- or 2-deoxyglucose-treated PC12D cells, also were observed in cells treated with memantine or clemastine, though not in cells treated with flunarizine (Figure 4C). These results suggested that two of these FDA-approved drugs, memantine and clemastine, are inducers of ER stress. Although flunarizine increased phosphorylation of EIF2S1 and DDIT3 expression, this increase was mediated by an EIF2AK3-independent pathway, indicating that flunarizine might induce the integrated stress response rather than ER stress [38].

SMK-17 induces autophagy in a MAP2 K/MEK-inhibition- or MTOR-independent manner

In the course of our primary screen (Figure 1F), we identified a novel autophagy inducer, SMK-17 (Figure 5A). SMK-17 induced the generation of MAP1LC3B-II/LC3-II (microtubule associated protein 1 light chain 3 beta, lipidated), an indicator of autophagosome formation [1]) in a time-dependent manner (Figure 5B). The LC3 conversion by SMK-17 was further
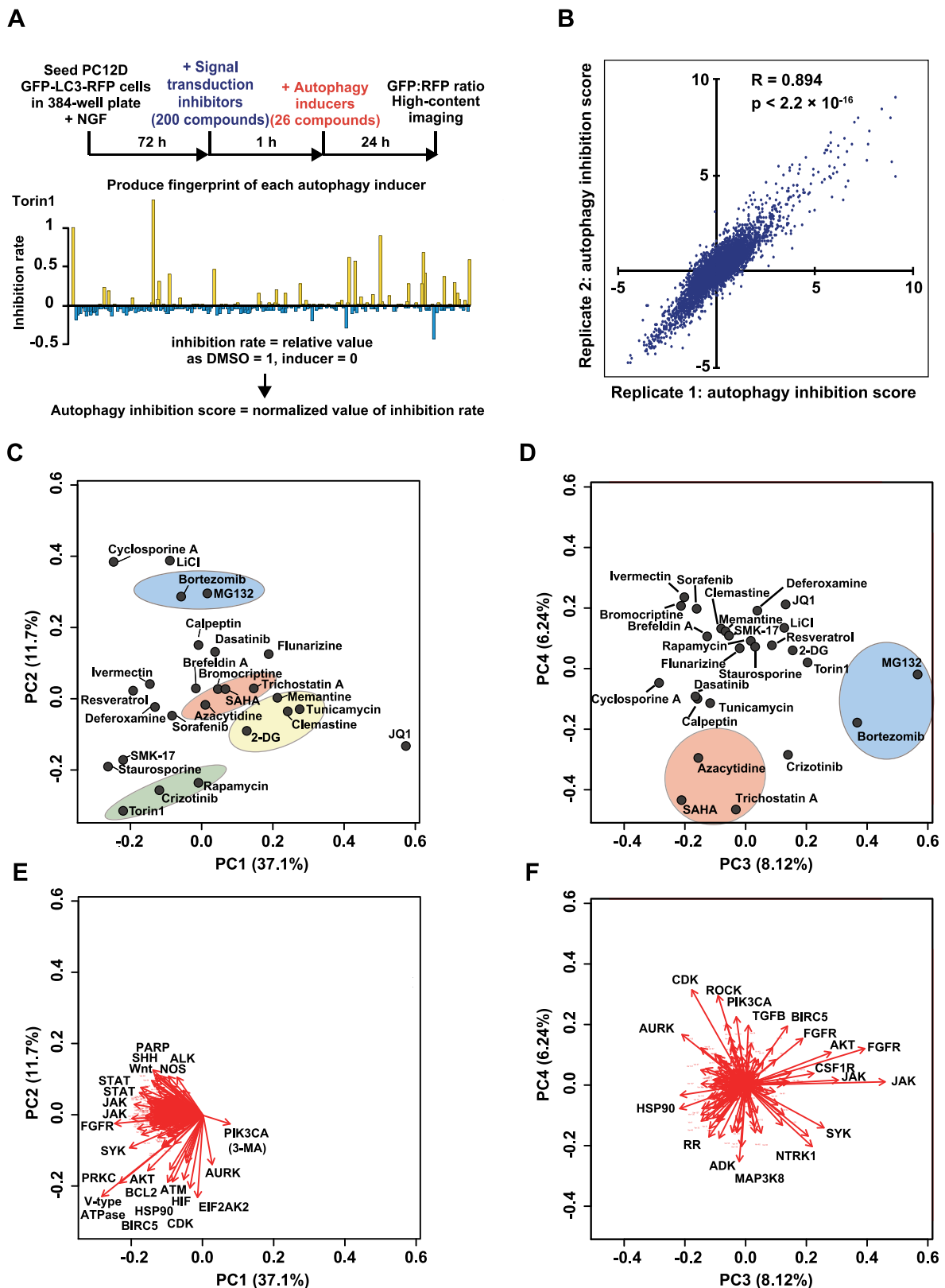
Figure 2. Chemical genomic analyses with principal component analysis (PCA). (A) Schematic illustration of the experiments for chemical genomic analyses. (B) Scatterplot of the two-independent datasets of autophagy inhibition scores, as used to confirm reproducibility. (C, D) Two-dimensional plot of PCA scores of (C) PC1 and PC2 and (D) PC3 and PC4, as analyzed by autophagy inhibition scores. (E, F) Loading plot of (E) PC1 and PC2 and (F) PC3 and PC4, from the PCA of autophagy inhibition scores.

increased in the presence of lysosomal inhibitor, bafilomycin A$_1$ (Figure 5C), indicating that SMK-17 activates autophagy flux. Consistently, the number of red dots were increased following exposure to SMK-17 in PC12D cells expressing a tandem

fluorescent label-tagged LC3 (mCherry-GFP-LC3, tfLC3 [39]), a well-established autophagic probe (Figure 5D). Given that SMK-17 originally was developed as a selective inhibitor of MAP2 K1/MEK1 and MAP2 K2/MEK2 (together as MAP2 K)
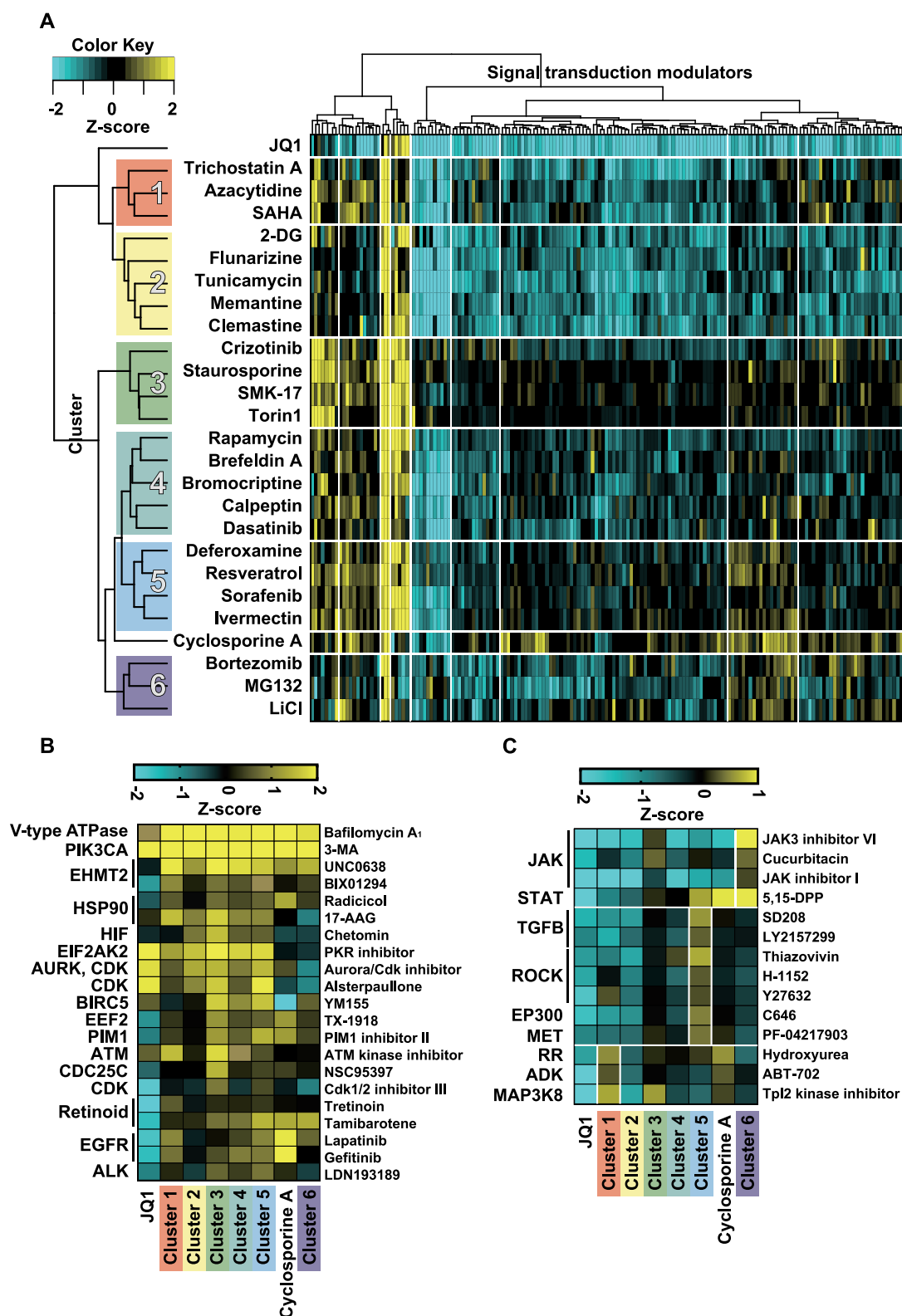
Figure 3. Clustering and heatmap analyses of autophagy inhibition patterns. (A) Hierarchical clustering and heatmap analyses of the chemosensitivity profiles of autophagy inhibition against 26 autophagy inducers. Hierarchical clustering analysis was performed using Euclidean distance and Ward's method. Rows indicate 170 different well-established compounds, and columns indicate 26 autophagy inducers. (B, C) Heatmap analyses of the autophagy profiles of the average of each cluster with the indicated signal transduction modulators. (**A, B, C**) The heatmap shows a gradient color scale ranging from cyan to black to yellow, indicating the autophagy inhibition score (z-score).

[40], we examined whether MAP2 K inhibition stimulates autophagy. As shown in Figure 5D,E, unlike other MAP2 K inhibitors (U0126 and PD184352), SMK-17 activated autophagosome formation and increased the number of red dots seen in PC12D cells expressing a tfLC3 probe, indicating that SMK-17 induced autophagy in a MAP2 K inhibition-independent manner. Given that SMK-17 clustered with torin1 by clustering analysis (Figure 3A), we next examined whether SMK-17 induces autophagy via the
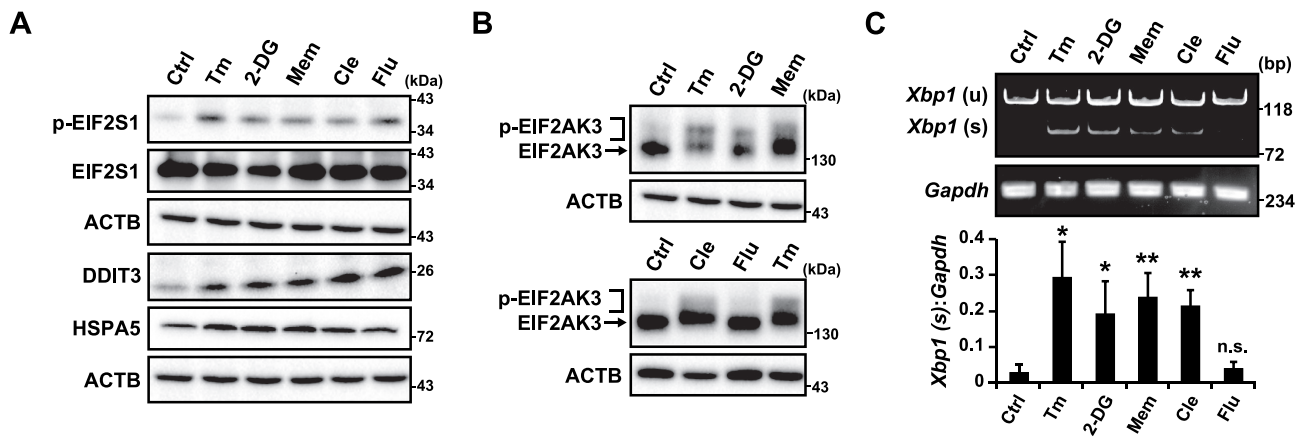
Figure 4. Memantine and clemastine induce ER stress. (A) Effect of memantine, clemastine, and flunarizine on the expression of ER stress markers. NGF-differentiated PC12D cells were treated with 2 μM tunicamycin (Tm), 10 mM 2-deoxyglucose (2-DG), 100 μM memantine (Mem), 5 μM clemastine (Cle), or 20 μM flunarizine (Flu). After 12 h (for detection of EIF2S1 phosphorylation) or 24 h (for detection of HSPA5 and DDIT3 expression), the cells were collected and subjected to western blotting analysis with the indicated antibodies. (B) Memantine and clemastine induce EIF2AK3 phosphorylation. NGF-differentiated PC12D cells were treated with the indicated compounds at the same concentrations as described in (A). After 12 h, the cells were collected and subjected to western blotting analysis with the indicated antibodies. (C) Memantine and clemastine induce alternative *Xbp1* mRNA splicing. NGF-differentiated PC12D cells were treated with the indicated compounds for 12 h at the same concentrations as described in (A). Unspliced (U) and spliced (S) *Xbp1* were detected by RT-PCR. Data are shown as mean ± SD (n = 3). n.s., non-significant, *$p < 0.05$, **$p < 0.01$ (two-tailed Student's t test).
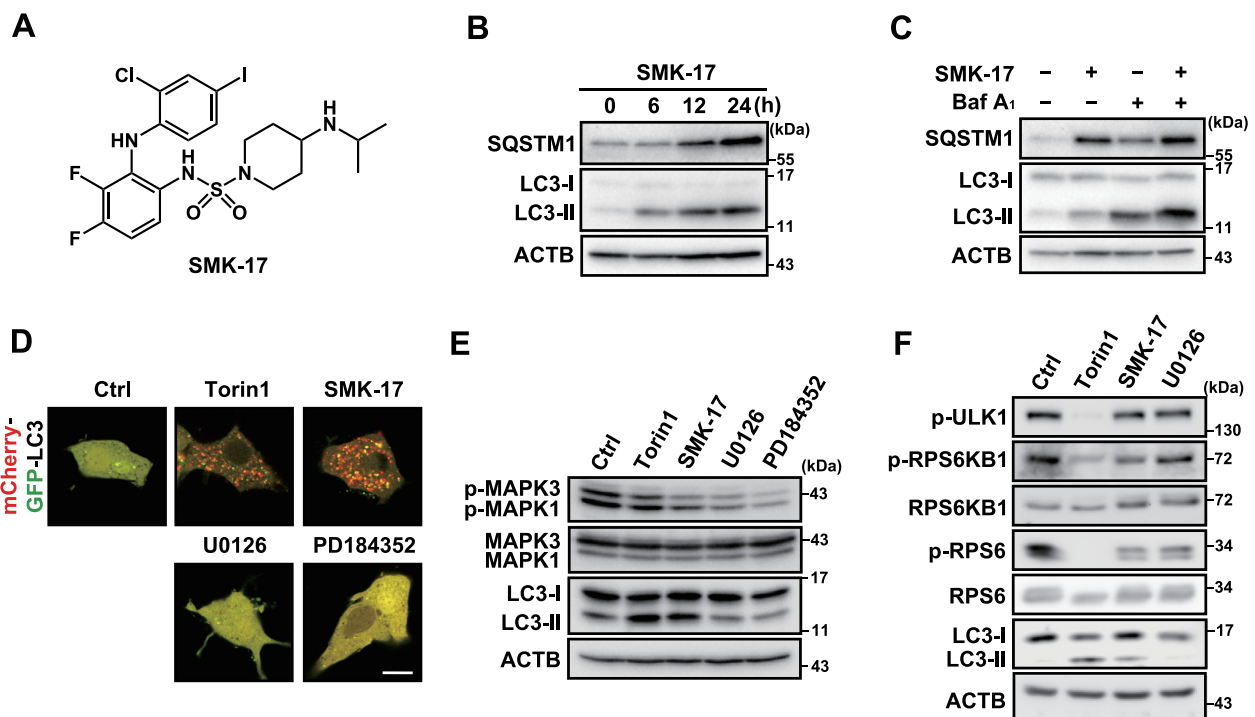
Figure 5. SMK-17 induces autophagy in a MAP2 K inhibition- or MTOR-independent manner. (A) Chemical structure of SMK-17. (B, C) Western blotting analyses of NGF-differentiated PC12D cells treated with (B) 10 μM SMK-17 for the indicated times, (C) 10 μM SMK-17 in the presence or absence of 100 nM bafilomycin A$_1$ (Baf A$_1$) for 24 h with the indicated antibodies. (D) NGF-differentiated PC12D cells transfected with the *mCherry-GFP-LC3* (tfLC3) plasmid vector were treated with 100 nM torin1, 10 μM SMK-17, 10 μM U0126, or 10 μM PD184352 for 8 h. Autophagy flux was observed under confocal microscopy. Scale bar: 20 μm. (E, F) Western blotting analyses of NGF-differentiated PC12D cells treated with (E) 100 nM torin1, 10 μM SMK-17, 10 μM U0126, or 10 μM PD184352 for 4 h, or (F) 100 nM torin1, 10 μM SMK-17, or 10 μM U0126 for 1 h with the indicated antibodies.

MTOR pathway. Torin1 suppressed the accumulation of p-RPS6/S6, p-RPS6KB1/S6K, and p-ULK1 (Figure 5F), effects known to reflect inhibition of MTOR [1]. SMK-17 also yielded attenuation of the level of p-RPS6, but not those of p-RPS6KB1 and p-ULK1 (Figure 5F), suggesting that SMK-17 induces autophagy via an MTOR-independent pathway. Given that U0126 also yielded attenuation of the levels of p-RPS6, we inferred that the decrease in p-RPS6 level following SMK-17 exposure reflects the inhibition of MAP2 K by SMK-17. SMK-17 increased the expression level of SQSTM1/p62 (sequestosome 1), an autophagy receptor, indicating that SMK-17 either inhibits autophagic degradation or transcriptionally upregulates the *Sqstm1* mRNA expression [1] (Figure 5B). Considering that SMK-17 enhanced autophagy flux measured by various
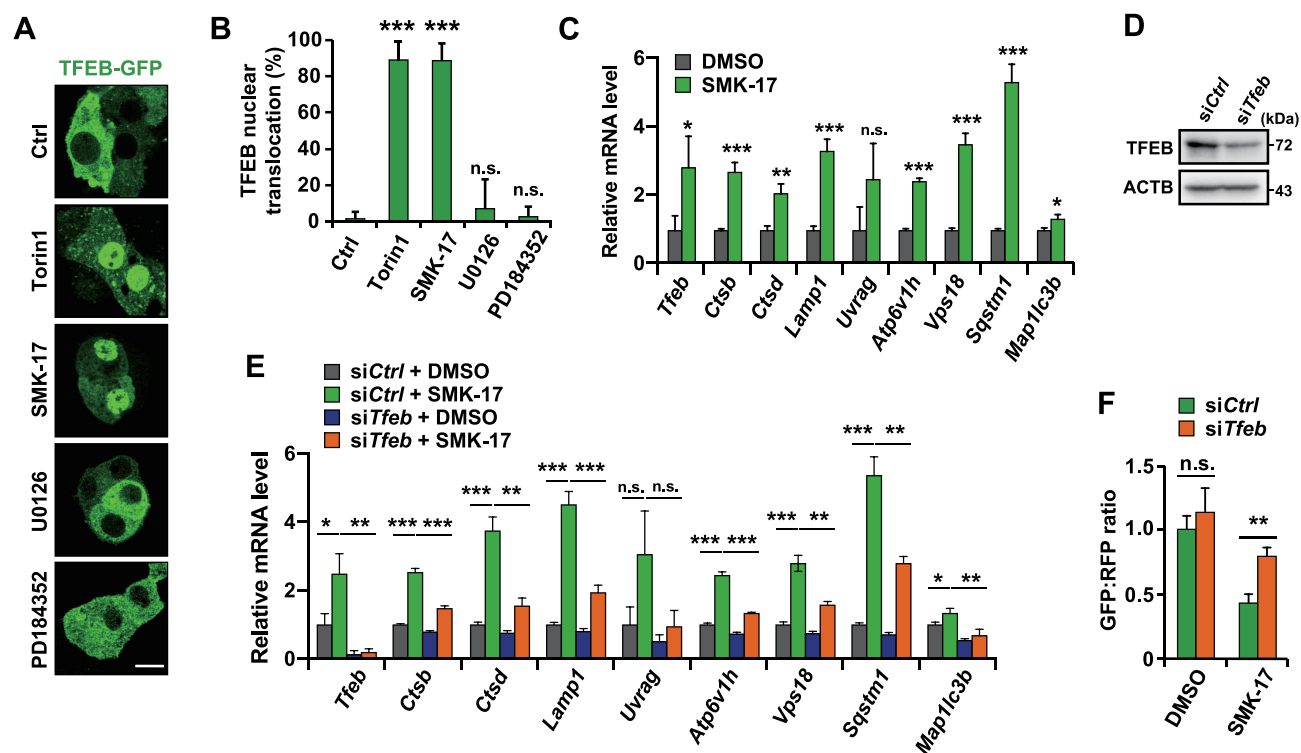
Figure 6. SMK-17 induces autophagy through TFEB activation. (A) Representative images and (B) quantification of TFEB nuclear translocation assay results. NGF-differentiated PC12D cells stably expressing TFEB-GFP were treated with 100 nM torin1, 10 μM SMK-17, 10 μM U0126, or 10 μM PD184352 for 1 h. (C, D, E) SMK-17 induces expression of TFEB target genes. (C) NGF-differentiated PC12D cells were treated with 10 μM SMK-17 for 6 h followed by qRT-PCR analysis. (D) Knockdown of TFEB in NGF-differentiated PC12D cells was confirmed with western blotting. (E) NGF-differentiated PC12D cells transfected with *Tfeb* siRNA or control siRNA were treated with 10 μM SMK-17 for 6 h followed by qRT-PCR analysis. (F) Involvement of TFEB in SMK-17-induced autophagy. NGF-differentiated PC12D cells expressing GFP-LC3-RFP were transfected with *Tfeb* siRNA or control siRNA and then treated with 10 μM SMK-17 for 24 h. Autophagy flux was evaluated by GFP:RFP ratio using a plate reader. Scale bar: 20 μm. Data are shown as mean ± SD (n = 3). n.s., non-significant, *p < 0.05, **p < 0.01, ***p < 0.001 (two-tailed Student's t test).

experiments (Figures 1F,5C,D), we expected that SMK-17 would transcriptionally increase the *Sqstm1* expression, and examined the possible involvement of TFEB, a master regulator of lysosomal/autophagy gene expression in SMK-17-induced autophagy [41–43].

SMK-17 induces TFEB nuclear translocation leading to autophagy activation

Interestingly, although SMK-17 apparently did not inhibit MTOR, the compound induced TFEB nuclear translocation leading to lysosomal/autophagy gene expression (Figure 6A, B), a process that is regulated primarily by MTOR [6]. Indeed, we found that SMK-17 induced upregulation of the expression of 9 well-known TFEB target genes including *Sqstm1* (Figure 6C). In addition, knockdown of TFEB (Figure 6D) significantly suppressed the SMK-17-induced expression of all these TFEB target genes (Figure 6E), and it also suppressed SMK-17-induced autophagy (Figure 6F). These results indicated that SMK-17 induced autophagy through TFEB-mediated lysosomal/autophagy gene expression.

SMK-17 activates PRKC/PKC-TFEB pathway leading to clearance of protein aggregates

A previous study showed that PRKC controls TFEB activity in an MTOR-independent manner [44]. Moreover, our chemical

genomic analysis revealed that a PRKC inhibitor counteracted SMK-17-induced autophagy (Figure 2C,E). Therefore, we examined the possible involvement of PRKC in the SMK-17-mediated autophagy pathway. We found that the phosphorylation levels of PRKC substrates were increased in SMK-17-treated cells as well as phorbol 12-myristate 13-acetate (PMA, PRKC activator)-treated cells (Figure 7A), and the increased phosphorylation of PRKC substrates by SMK-17 treatment was abrogated by PRKC inhibitor Gö6983 (Figure 7B), indicating that SMK-17 enhances PRKC activity. Moreover, TFEB nuclear translocation induced by SMK-17 was strongly suppressed by the PRKC inhibitor, although this PRKC inhibitor did not affect torin1-induced TFEB nuclear translocation (Figure 7C,D), indicating that SMK-17-induced TFEB nuclear localization is regulated by PRKC signaling. TFEB nuclear translocation is expected to induce lysosomal biogenesis [6], and SMK-17 or torin1 induced lysosomal biogenesis as judged from the increased LysoTracker DND-99 signal intensity, an indicator of acidic organelles including lysosomes. This effect induced by SMK-17 was suppressed by PRKC inhibition, while the increased signal intensity of LysoTracker by torin1 treatment was not affected by PRKC inhibition (Figure 7E,F). Consistently, this PRKC inhibitor inhibited SMK-17-induced autophagy, but not torin1-induced autophagy (Figure 7G). These results indicated that SMK-17 induces autophagy and lysosomal biogenesis via MTOR-independent but PRKC-dependent TFEB activation.
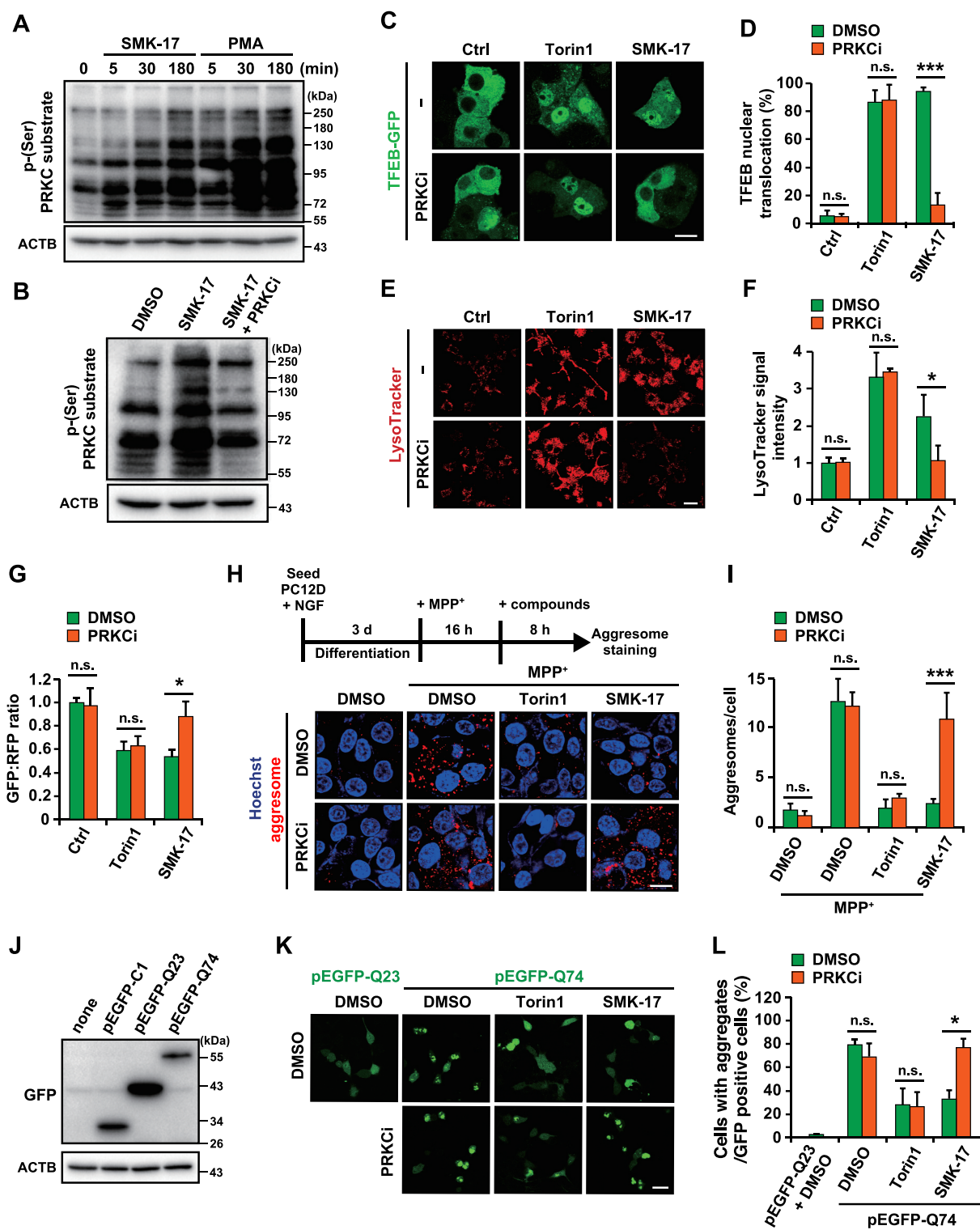
Figure 7. SMK-17 induces PRKC/PKC-dependent TFEB activation and clearance of intracellular aggregates. (A, B) Western blotting analyses of NGF-differentiated PC12D cells treated with (A) 10 µM SMK-17 or 100 nM phorbol 12-myristate 13-acetate (PMA) for the indicated times, or (B) 10 µM SMK-17 in the presence or absence of 5 µM PRKC inhibitor (PRKCi, Gö6983) for 3 h. Phosphorylation of PRKC substrates was detected by using p-(Ser) PRKC substrate antibody. (C) Representative images and (D) quantification of TFEB nuclear translocation assay results. NGF-differentiated PC12D cells stably expressing TFEB-GFP were treated with 100 nM torin1 or 10 µM SMK-17 in the presence or absence of 5 µM PRKCi. Scale bar: 20 µm. (E) Representative images and (F) quantification of LysoTracker Red DND-99 staining assay results. NGF-differentiated PC12D cells were treated with 100 nM torin1, 10 µM SMK-17 in the presence or absence of 5 µM PRKCi. Mean fluorescent intensity was quantified. Scale bar: 20 µm. (G) NGF-differentiated PC12D cells expressing GFP-LC3-RFP were treated with 100 nM torin1 or 10 µM SMK-17 for 24 h in the presence or absence of 5 µM PRKCi. Autophagy flux was evaluated by GFP:RFP ratio using a plate reader. (H) Representative images and (I) quantification of aggresome clearance assay results. NGF-differentiated PC12D cells were treated with MPP$^+$ for 16 h prior to treatment with 100 nM torin1 or 10 µM SMK-17 for 8 h in the presence or absence of 5 µM PRKCi. The number of aggresoe dots per cell in each image was quantified. Scale bar: 20 µm. (J) Western blotting analysis of NGF-differentiated PC12D cells transiently transfected with GFP, GFP-HTTQ23, or GFP-HTTQ74 for 72 h. (K) Representative images and (L) quantification of mutant HTT clearance assay results. NGF-differentiated PC12D cells were transiently transfected with GFP-HTTQ23 or GFP-HTTQ74 for 48 h prior to treatment with 100 nM torin1 or 10 µM SMK-17 for 24 h in the presence or absence of 5 µM PRKCi. Percentage of cells with GFP-HTT aggregates to GFP-positive cells was calculated in each sample. Data are shown as mean ± SD (n = 3). n.s., non-significant, *p < 0.05, ***p < 0.001 (two-tailed Student's t test).

Accumulation of aggregated proteins is associated with various diseases including neurodegenerative disorders such as PD and HD. Autophagy induction has been proposed as a new strategy for the treatment of proteinopathies by removing cytotoxic aggregates or damaged organelles [3]. Therefore, we examined whether autophagy activation by SMK-17 resulted in the depletion of protein aggregates. We previously observed that the treatment with 1-methyl-4-phenylpyridinium (MPP$^+$), a compound widely used to induce cellular and animal models of PD, causes aggresome formation [45]. In the present work, we observed that SMK-17 induced the clearance of aggresomes formed in PC12D cells and human neuroblastoma SH-SY5Y cells pre-treated with MPP$^+$. Notably, the aggresome-clearing effect of SMK-17 was significantly abrogated in the presence of a PRKC inhibitor (Figure 7H,7I, S2A, and S2B). We also tested the efficacy of SMK-17 in a cellular model of HD induced by overexpression of EGFP-tagged HTT (huntingtin) exon1 containing 74 polyQ repeats (EGFP-HTTQ74), which is a well-established autophagy receptor [4] (Figure 7J). As a result, transfection with EGFP-HTTQ74 but not wild type 23 polyQ repeats (EGFP-HTTQ23) caused aggregation in neuronal PC12D cells (Figure 7K,L). HTTQ74 aggregation was suppressed by not only SMK-17 but also torin1, and PRKC inhibitor remarkably inhibited only SMK-17-mediated clearance of HTTQ74 aggregates (Figure 7K,L). Taken together with these results, we propose that SMK-17 induces clearance of protein aggregates by activating autophagy via the PRKC-TFEB pathway.

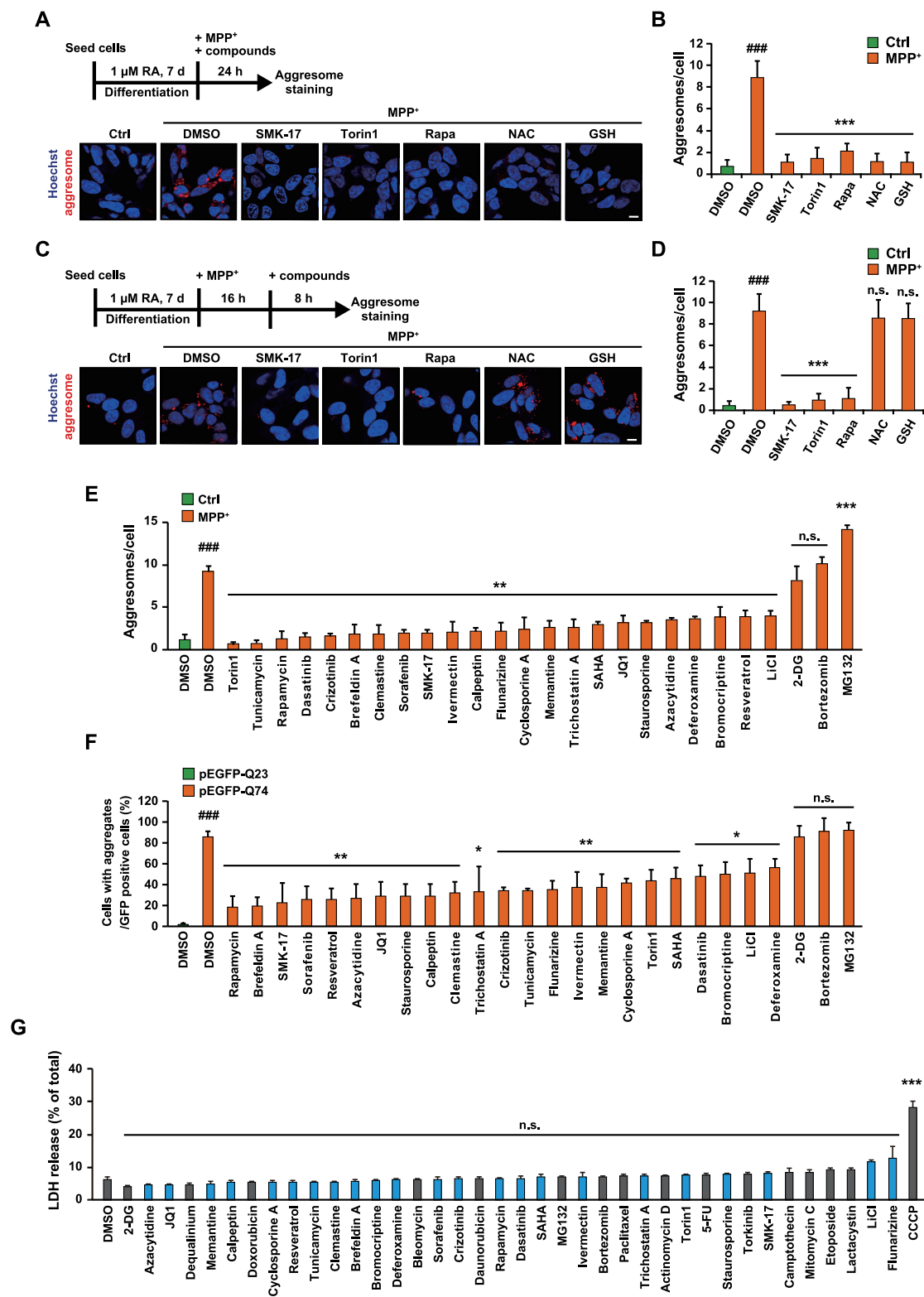### Clearance activity of protein aggregates by autophagy-inducing small molecules

PD is pathologically associated with the interrelated processes of abnormal protein accumulation and oxidative stress due to mitochondrial dysfunction [46]. Indeed, we found that the well-known antioxidants N-acetylcysteine (NAC) and glutathione (GSH) as well as the autophagy inducers SMK-17, torin1, and rapamycin significantly inhibited aggresome formation when provided simultaneously with MPP$^+$ (Figure 8A, B). In contrast, although autophagy inducers also provided significant clearance of aggresomes in cells pre-treated with MPP$^+$, NAC and GSH did not (Figure 8C,D). These results indicated that autophagy induction is required for clearance of aggregated proteins in our cellular models of PD. To confirm this inference, 26 small molecules identified as autophagy inducers were assessed for their aggresome clearance activity. Notably, almost all of the autophagy inducers (excepting 2-deoxyglucose and two proteasomal inhibitors, MG132 and bortezomib) yielded significant attenuation of aggresome accumulation (Figure 8E and S3A). Similarly, these autophagy inducers significantly induced the clearance of mutant HTT (Figure 8F and S3B). Finally, we evaluated the cytotoxicity of autophagy inducers tested in this study against more appropriate cells derived from neural tissues than PC12D cells. We found that 23 autophagy inducers, which induced the clearance of protein aggregates, did not show cytotoxicity against primary cultured rat cortical neurons as judged from LDH assay (blue bars, Figure 8G). Interestingly, other autophagy inducers including cytotoxic compounds against PC12D cells, except for CCCP, also did not affect cell viability in primary cultured rat cortical neurons (black bars, Figure 8G). These results suggested that stimulation of autophagy removes protein aggregates without neurotoxicity, implying on a potential indication of treatment against neurodegenerative diseases with neuronal aggregations.

Discussion

In this study, we addressed the induction of autophagy by small molecules. To this end, we used a chemical genomic technique previously employed for several studies that identified diverse and selective signaling pathways involved in cancer cell migration and ER stress response [9,47]. Among the 39 autophagy inducers identified by our initial chemical screen, 13 compounds were excluded from further investigation because of their cytotoxicity in PC12D cells (**Fig. S1**). The remaining 26 compounds were subjected to chemical genomic analysis to profile the pattern of autophagy induction. Based on the results of PCA and clustering analysis, the autophagy inducers were classified into several groups, possibly reflecting distinct modes of action. Considering the effect of signal transduction inhibitors on autophagy induction, JAK, STAT (signal transducer and activator of transcription); TGFB1, ROCK1, EP300 (E1A binding protein p300); and ADK, RR, MAP3K8 signaling were inferred to be involved in the autophagy induced by compounds within (respectively) Clusters 6, 5, and 1 (Figure 3C). This finding may provide a clue for mechanistic analysis of the autophagic processes induced by those compounds. Unfortunately, we did not identify specific pathways associated with the differences among Clusters 2, 3, and 4 (Figure 3A). However, we hypothesize that similarities in the patterns of the autophagy profiles may be associated with overlapping mechanisms of autophagy induction. Next, we asked whether autophagy inducers in Clusters 3 and 4 inhibit MTOR, given that torin1 and rapamycin were classified into Clusters 3 and 4, respectively. Like torin1, SMK-17, staurosporine, and crizotinib are members of Cluster 3 and yielded attenuation of p-RPS6 levels; however, SMK-17, staurosporine, and crizotinib did not yield changes in the levels of p-ULK1, in contrast to torin1 (**Fig. S4A**). On the other hand, brefeldin A, bromocriptine, calpeptin, and dasatinib did not yield attenuation of either p-RPS6 or p-ULK1 levels, in contrast to rapamycin, although all 5 of these compounds were assigned to Cluster 4 (**Fig. S4B**). These results suggested that these compounds did not inhibit MTOR, and the difference between Clusters 3 and 4 may reflect distinct effects on p-RPS6 accumulation.

Our clustering analysis led to the finding that memantine and clemastine (Cluster 2) induced ER stress. Memantine is known as an antagonist of the N-methyl-D-aspartate (NMDA) receptor. Memantine and its structural analog amantadine have proven efficacy against Alzheimer disease [48] and PD [49], respectively. Recently, Hirano et al. [10] reported that memantine enhances autophagic flux, leading to the enhanced clearance of aggregation-prone proteins and damaged mitochondria in various neuronal models. However, memantine-induced autophagy is not dependent

Figure 8. Activities of autophagy inducers in inhibition of aggresome formation and clearance of protein aggregates. (A) Representative images and (B) quantification of aggresome formation assay results. RA-differentiated SH-SY5Y cells were treated with MPP$^+$ for 24 h in the presence or absence of 10 μM SMK-17, 100 nM torin1, 10 μM rapamycin, 10 mM NAC, or 10 mM GSH. The number of aggresome dots per cell in each image was quantified. Scale bar: 10 μm. (C) Representative images and (D) quantification of aggresome clearance assay results. RA-differentiated SH-SY5Y cells were treated with MPP$^+$ for 16 h prior to treatment with 10 μM SMK-17, 100 nM torin1, 10 μM rapamycin, 10 mM NAC, or 10 mM GSH for 8 h. The number of aggresome dots per cell in each image was quantified. Scale bar: 10 μm. (E) Quantification of the aggresome clearance assay results. RA-differentiated SH-SY5Y cells were treated with MPP$^+$ for 16 h prior to treatment with the indicated compounds for 8 h. See also Table 1 and **Fig. S3A**. The number of aggresome dots per cell in each image was quantified. (F) Quantification of the mutant HTT clearance assay results. NGF-differentiated PC12D cells were transiently transfected with GFP-HTTQ23 or GFP-HTTQ74 for 48 h prior to treatment with the indicated compounds for 24 h. See also **Table 1** and **Fig. S3B**. Percentage of cells with GFP-HTT aggregates to GFP-positive cells was calculated in each sample. (G) Cytotoxicity of the autophagy inducers against primary cultured rat cortical neurons. Cells were treated with the indicated compounds for 24 h, and cytotoxicity was measured by LDH release assay. The data are expressed as a percentage of total amount of LDH analyzed in each plate. Data are shown as mean ± SD (n = 3 [**B, D, E, F**], n = 5 [**G**]). $^{###}$p < 0.001 (two-tailed Student's t test compared to untreated control [Ctrl]). n.s., non-significant, *p < 0.05, **p < 0.01, ***p < 0.001 (two-tailed Student's t test [**B, D, E, F**], one-way ANOVA with post hoc Dunnett's test [**G**]).

on antagonism of the NMDA receptor [10]. In the present work, we demonstrated that memantine induced autophagy possibly through ER stress induction. Memantine inhibits the NMDA receptor with an IC_{50} of approximately 1 µM; however, higher concentrations (10–500 µM) of memantine affect many additional targets, including SIGMAR1 (sigma non-opioid intracellular receptor 1) [50]. Since SIGMAR1 is a chaperone protein residing at the mitochondrion-associated ER membrane, the inhibition of the SIGMAR1 is expected to inhibit ER function [51]. Indeed, another SIGMAR1 antagonist, haloperidol, has been reported to induce ER stress [52]. Therefore, it is likely that 100 µM memantine induces ER stress, possibly due to the inhibition of SIGMAR1 function. Once ER stress responses are activated, ERN1, a sensor of ER stress, could form a complex with TRAF2 (TNF receptor associated factor 2) and MAP3 K5/ASK1 (mitogen-activated protein kinase kinase kinase 5), causing activation of the MAPK8/JNK (mitogen-activated protein kinase), which in turn promotes autophagy via activation of BECN1 [53,54]. Activated ERN1 also activates the XBP1 transcription factor via unconventional splicing, and the activated XBP1 then regulates transcription of the BECN1-encoding gene through direct binding to the gene's promoter region [55]. As a result, BECN1 (upregulated by ER stress) forms a complex with PIK3C3 (phosphatidylinositol 3-kinase catalytic subunit type 3) and PIK3R4 (phosphoinositide-3-kinase regulatory subunit 4), triggering autophagosome formation [8]. Indeed, memantine has been reported to influence PIK3 C3 or components of the PIK3 C3 complex [10]. Clemastine (Tavegil™), an antihistamine drug originally marketed for the treatment of allergic rhinitis, has efficacy against multiple sclerosis [56]. Recently, clemastine was also was shown to be capable of counteracting spinal cord pathology and neuroinflammatory responses in the SOD1^{G93A} (superoxide dismutase 1) mouse model of amyotrophic lateral sclerosis [57]. In addition, clemastine has been reported to activate autophagy in SOD1^{G93A} primary microglia [58]. The stimulation of autophagy by clemastine is consistent with the role that H1-targeting antihistamines play in autophagy [11,59]. Among several histamine H1 receptor antagonists, astemizole has been reported to induce ER stress and autophagy, possibly through the accumulation of intracellular Ca^{2+} [60]. Moreover, terfenadine, another histamine H1 antagonist, also has been shown to potentiate the concentration of cytosolic Ca^{2+} and to induce autophagy [11,61]. Therefore, we infer that clemastine also induces ER stress through increases in cytosolic Ca^{2+}, leading in turn to autophagy induction.

Flunarizine, which also was classified into Cluster 2 in our analysis, is a voltage-dependent L-/T-type Ca^{2+} channel blocker that is approved for treating migraine and epilepsy. Moreover, flunarizine has been reported to alter autophagy [62]. Although flunarizine did not induce ER stress, as assessed by the failure of the compound to induce EIF2AK3 phosphorylation, flunarizine induced activation of the EIF2S1-ATF4 (activating transcription factor 4)-DDIT3 pathway, which is commonly observed with other ER stress inducers classified into Cluster 2. Several genes, including those

encoding ATG5 (autophagy related 5), ATG12 (autophagy related 12), and SQSTM1, have been reported to be transcriptionally regulated by the EIF2S1-ATF4-DDIT3 pathway [63,64]. There are four EIF2S1 kinases (EIF2AK1/HRI, EIF2AK2, EIF2AK3, EIF2AK4/GCN2 [eukaryotic translation initiation factor 2 alpha kinase 1–4]), all of which are activated in response to various stimuli [65]. Therefore, we propose that flunarizine induces activation of the EIF2S1-ATF4-DDIT3 pathway via EIF2S1 kinases other than EIF2AK3, thereby leading to autophagy induction.

In the course of the screen, we identified a novel autophagy inducer, SMK-17. SMK-17 originally was developed as a MAP2 K inhibitor that exerts potent antitumor effects both *in vitro* and *in vivo* [40,66]. However, unlike SMK-17, two other MAP2 K inhibitors (U0126 and PD184352) did not activate autophagy flux in PC12D cells, indicating that SMK-17 induces autophagy in a MAP2 K inhibition-independent manner. On the other hand, trametinib, an inhibitor of MAP2 K, has been reported to activate autophagy in pancreatic ductal adenocarcinoma (PDA) cells, in which the KRAS-RAF-MAP2 K-MAPK/ERK pathway is activated [67]. These results indicate that the KRAS-RAF-MAP2 K-MAPK/ERK pathway may regulate autophagy, depending on the status of the cultured cells under study. Mechanistically, trametinib treatment of PDA cells led to decreased phosphorylation of STK11/LKB1 (serine/threonine kinase 11) and increased phosphorylation of AMP-activated protein kinase (AMPK; at T172) and ULK1 (at S555) [67], indicating that trametinib-induced autophagy in PDA cells is mediated by the STK11-AMPK-ULK1 signaling axis. On the other hand, SMK-17 failed to inhibit phosphorylation of the autophagy-negative regulation site of ULK1 (residue S757), indicating that SMK-17-induced autophagy in PC12D cells is mediated by a pathway distinct from the STK11-AMPK-ULK1 signaling axis. PCA of our chemical genomic data predicted the involvement of PRKC in SMK-17-induced autophagy. Indeed, we found that SMK-17 activated PRKC and induced TFEB nuclear translocation (thereby activating lysosomal biogenesis and autophagy) in a PRKC-dependent manner. According to previous reports, PRKC activates MAPK/JNK and MAPK14/p38, in turn inactivating ZKSCAN3 (zinc finger with KRAB and SCAN domains 3), a repressor of lysosomal/autophagy genes [44,68]. Moreover, some isotypes of PRKC also are regulated by PDPK1 (3-phosphoinositide dependent protein kinase 1) [69]. Our chemical genomic study revealed that MAPK/JNK, MAPK14/p38 inhibitors and a PDPK1 (3-phosphoinositide dependent protein kinase 1) inhibitor, as well as a PRKC inhibitor, counteracted SMK-17-induced autophagy (**Fig. S5**). At present, we do not know the mechanism of SMK-17-induced PRKC activation, but SMK-17 nonetheless appears to induce autophagy through PRKC.

Autophagy has an essential role in eliminating nonfunctional and potentially cytotoxic aggregation-prone proteins. Therefore, the stimulation of autophagy with small molecules may serve as a new therapeutic strategy for proteinopathies including PD, which is characterized by the accumulation of aggregated proteins ("Lewy bodies"). Oxidative stress due to mitochondrial dysfunction is closely associated with PD and is a major cause of protein aggregation [70,71]. We previously

observed that MPP$^+$, a neurotoxin known to act as an inhibitor of mitochondrial complex I, induces reactive oxygen species (ROS) and aggresome formation in neuronal PC12D cells [45]. Indeed, the potent antioxidants NAC and GSH significantly suppressed MPP$^+$-induced aggresome formation. However, NAC and GSH failed to induce the clearance of aggresomes formed by pre-treatment with MPP$^+$, indicating that antioxidant molecules can only inhibit aggresomes at the formation stage. On the other hand, almost all of the autophagy-inducing compounds tested in the present study (with the exception of proteasome inhibitors and 2-deoxyglucose) provided aggresome clearance. Although proteasome inhibitors have been reported to impair autophagy [72,73], our findings that proteasome inhibitors activated autophagy are consistent with a recent report that proteasome inhibitors induced autophagy [74]. Considering the ubiquitin-proteasome system is also involved in protein degradation pathway [75], aggresome accumulation has been inferred to be the result of proteasome inhibition. 2-Deoxyglucose exposure mimics glucose deprivation, a process that causes oxidative stress and stimulates aggresome formation in cardiac myocytes [76], suggesting that 2-deoxyglucose enhances aggresome formation while activating autophagy.

In summary, our chemical genomic approach was able to classify autophagy inducers into several clusters that appeared to correlate with their autophagy-inducing mode of action. Analysis of individual clusters led to the demonstration (the first, to our knowledge) that memantine and clemastine, compounds approved by the FDA for the treatment of neurodegenerative disease, may function through the activation of ER stress-mediated autophagy. Therefore, the chemical genomic approach is expected to be useful for the functional analysis of approved drugs and for development of repositioned drugs. Moreover, our combined chemical genomic and PCA approach permitted us to identify SMK-17 as a new autophagy inducer that induces autophagy via PRKC activation. In addition, we demonstrated that autophagy inducers provide the clearance of protein aggregates in cellular models of PD and HD without showing any cytotoxic effect on primary cultured rat cortical neurons, suggesting that autophagy induction may improve neuronal function in patients with PD or HD (as well as those with other proteinopathies) even after disease onset.

Materials and Methods

Reagents and antibodies

SCADS inhibitor kits were supplied by the Molecular Profiling Committee, Grant-in-Aid for Scientific Research on Innovative Areas "Advanced Animal Model Support (AdAMS)", from the Ministry of Education, Culture, Sports, Science and Technology, Japan (KAKENHI 16H06276). Staurosporine was prepared from one such kit. 2-Deoxy-D-glucose (D6134), bromocriptine (B2134), crizotinib (PZ0191), dasatinib (SML2589), deferoxamine (D9533), ivermectin (I8898), JQ1 (SML1524), resveratrol (R5010), SAHA (SML0061), and MPP$^+$ (D048) were purchased from Sigma-Aldrich. Bortezomib (S1013) and calpeptin (S7396) were purchased from Selleck Biotech. All-trans retinoic acid (RA, 182–01111),

azacytidine (016–25361), cyclosporine A (031–24931), GSH (071–02014), lithium chloride (123–01162), memantine hydrochloride (41100–52-1), NAC (015–05132), trichostatin A (203–17561), and tunicamycin (202–08241) were purchased from FUJIFILM Wako Pure Chemical Corporation. Brefeldin A (203729) was purchased from Calbiochem. MG132 (10012628) and torin1 (10997) were purchased from Cayman Chemical. Rapamycin (R-5000) was purchased from LC Laboratories. Clemastine fumarate (C568500) was purchased from Toronto Research Chemicals. Flunarizine hydrochloride (0522/500) was purchased from Tocris Bioscience. SMK-17 and sorafenib were kindly provided by the Daiichi-Sankyo Pharmaceutical Company. Gö6983 (ab144414) and phorbol 12-myristate 13-acetate (PMA, ab120297) were purchased from Abcam. Nerve growth factor 2.5S (NGF; N-100) was purchased from Alomone Labs. Antibodies were obtained as follows: anti-ACTB/β-actin (A1978) and anti-LC3 (L7543) from Sigma-Aldrich; anti-p-ULK1 (6888), anti-p-RPS6KB1/S6 K (9204), anti-RPS6 KB1/S6 K (9202), anti-p-RPS6/S6 (4858), anti-RPS6/S6 (2217), anti-p-MAPK/ERK (9101), anti-MAPK/ERK (9102), anti-p-EIF2S1/eIF2α (ser51) (9721), anti-EIF2S1/eIF2α (9722), anti-EIF2AK3/PERK (3192), anti-SQSTM1/p62 (5114), and anti-p-(Ser) PRKC/PKC substrate (2261) from Cell Signaling Technology; anti-DDIT3/CHOP (MA1-250) from Thermo Fisher Scientific; anti-KDEL (ENZ-ABS679), used for HSPA5/GRP78 detection, from Enzo Life Sciences; and anti-TFEB (13372-1-AP) from proteintech.

Cell culture

All cells were cultured at 37°C in a 5% CO$_2$ environment. Rat adrenal pheochromocytoma PC12D cells [77] (obtained from Dr. Kazuo Umezawa at Keio University) were cultured in Dulbecco's modified Eagle medium (DMEM; Nissui Pharmaceutical, 05919) supplemented with 5% fetal bovine serum (Equitech-Bio, SFBU30), 10% horse serum (Nippon Bio-Test Laboratories, 0204–2), 0.6 mg/mL L-glutamine (Sigma-Aldrich, G8540), 100 U/mL penicillin G (Sigma-Aldrich, P3032), and 0.1 mg/mL kanamycin (Sigma-Aldrich, K1377). Human neuroblastoma SH-SY5Y cells (ATCC, CRL-2266) were cultured in DMEM supplemented with 10% fetal bovine serum, L-glutamine, and antibiotics. Differentiation was achieved by 72 h treatment with 100 ng/mL NGF (for PC12D) or 7 d treatment with 1 μM RA (for SH-SY5Y).

siRNA transfection

Stealth siRNA against *Tfeb* (RSS337388) and negative control siRNAs (12935300) were purchased from Invitrogen. Cells were transfected with 100 nM siRNA using Lipofectamine RNAiMAX (Invitrogen, 13778075) for 48 h.

Plasmid transfection

To generate tfLC3 vector, sequences encoding mCherry and human LC3B were inserted into the pEGFP-C1 plasmid vector (Clontech, 6084–1). pEGFP-N1-TFEB (38119, Dr. Shawn Ferguson's lab) was purchased from Addgene. EGFP-tagged HTT exon1 (pEGFP-Q23 or pEGFP-Q74) has been described

previously [10]. Transfections were performed with Lipofectamine 3000 (Invitrogen, L3000008) according to the manufacturer's protocol unless otherwise stated.

Retroviral transduction

GFP-Lc3-RFP was amplified by PCR from the pMRX-IP-GFP-LC3-RFP (gift from Dr. Noboru Mizushima at the University of Tokyo) plasmid vector [13] using the following primers: forward, CTCTAGACTGCCGGATCCCCCGCCGCCACC; reverse, AGGAATTCCCGTACCACCACACTGGGATCC. *GFP-Lc3-RFP* then was cloned into the BamHI site of the pGCDNsam vector (generated as described previously [78]). For the generation of retrovirus, the resulting pGCDNsam-*GFP-Lc3-RFP* plasmid was co-transfected with pVSV-G vector (Clontech, 631530) into GP2-293 (Clontech, 631530) cells using Lipofectamine LTX (Invitrogen, 15338100). Maintenance of GP2-293 cells and plasmid transfection were performed according to the manufacturer's protocol. 293GPG cells [79] were maintained according to the method described elsewhere [78], and transduced by exposure to viral supernatants harvested from the GP2-293 culture supernatants harvested on days 1, 2, and 3 with 4 μg/mL of polybrene by spinoculation at 1000 × g for 1 h at 32°C followed by cell sorting using FACSAria III (BD Biosciences, San Jose, CA) to enrich for 293GPG cells stably expressing GFP-LC3-RFP. Virus supernatant from 293GPG-GFP-LC3-RFP cells was harvested and concentrated as described [78]. PC12D cells stably expressing GFP-LC3-RFP cells were generated by transduction and sorting as above, using the concentrated virus from 293GPG-GFP-LC3-RFP cells.

Autophagy flux assay

For ratiometric autophagy flux assay, PC12D-GFP-LC3-RFP cells were seeded into a 384-well black plate (CellCarrier 384-Ultra; PerkinElmer, 6057308). After 72 h differentiation by exposure to 100 ng/mL NGF, cells were treated with compounds for 24 h. Cells were then fixed with 10% formalin containing 2 μg/mL Hoechst33342 (Invitrogen, H3570) for 30 min. Image capture and quantification of GFP and RFP intensity in cells were performed using a high-content imager, OPERA Phenix and Harmony software ver 4.5 (PerkinElmer, Waltham, MA), or a plate-reader, SAFIRE (TECAN, Männedorf, Switzerland). For the autophagy flux assay using fluorescence imaging with tfLC3, NGF-differentiated PC12D cells were transfected with the tfLC3 vector. At 48 h after transfection, cells were treated with the indicated compounds for 8 h. Fixation, confocal microscopy was then performed as previously described [80].

PCA, clustering, and heatmap analyses

The rate of inhibition by each signal transduction modulator was calculated by setting the average of vehicle-treated cells at 1 and autophagy inducer-treated cells at 0. The autophagy inhibition score was then calculated by z-score normalization and analyzed by PCA, heatmap, and hierarchical clustering (based on Euclidean distance matrix and Ward's linkage method) using R ver 3.4.2 (http://www.R-project.org).

Western blotting analysis

Western blotting was performed according to a previously published method [81]. In brief, cells were lysed with RIPA buffer (Sigma-Aldrich, R0278) supplemented with protease inhibitor cocktail (Thermo Scientific, 78429), and protein lysates were loaded into SDS-PAGE gels (separating gels: 6.5–15% acrylamide/N,N'-methylenebis(acrylamide) 29:1 [FUJIFILM Wako Pure Chemical Corporation, 015–25635], 0.375 M Tris pH 8.8 [FUJIFILM Wako Pure Chemical Corporation, 514–37061], 0.1% w:v SDS [FUJIFILM Wako Pure Chemical Corporation, 191–07145], 0.1% v:v ammonium peroxodisulfate [FUJIFILM Wako Pure Chemical Corporation, 012–20503], and 0.0625% v:v N,N,N',N'-tetramethylethylenediamine [FUJIFILM Wako Pure Chemical Corporation, 205–06313]; stacking gels: 4% acrylamide/N,N'-methylenebis(acrylamide) 29:1 [FUJIFILM Wako Pure Chemical Corporation, 015–25635], 0.125 M Tris pH 6.8 [FUJIFILM Wako Pure Chemical Corporation, 2106–100], 0.1% w:v SDS [FUJIFILM Wako Pure Chemical Corporation, 191–07145], 0.075% v:v ammonium peroxodisulfate [FUJIFILM Wako Pure Chemical Corporation, 012–20503], and 0.25% v:v N,N,N',N'-tetramethylethylenediamine [FUJIFILM Wako Pure Chemical Corporation, 205–06313]) and transferred onto PVDF membranes (Millipore, IPVH00010). The membranes were incubated overnight at 4°C with the primary antibodies, and then incubated for 1 h at room temperature with the appropriate HRP-conjugated secondary antibodies. Chemiluminescence was detected using the Immobilon Western Kit (Merck Millipore, WBKLS0500) and ChemiDoc XRS+ (BioRad, Hercules, CA).

RNA extraction, RT-PCR, and Quantitative RT-PCR

Total RNA was extracted from NGF-differentiated PC12D cells using the RNeasy Plus Mini Kit (QIAGEN, 74136). From 2 μg of total RNA, first-strand complementary DNA (cDNA) was produced using M-MLV reverse transcriptase (Promega, M1701) according to the manufacturer's instructions. For detection of *Xbp1* splicing, first-strand cDNA from PC12D cells was subjected to PCR with KOD plus polymerase (Toyobo, KOD-201) using primers as follows: for *Xbp1*, AGTGGAGTAAGGCTGGTGGCC and CAACAGTGTCAGAGTCCATGGG; for *Gapdh*, TGTGATGGGTGTGAACCAC and GGATGCAGGGATGATGTTCT. The amplified products were separated by electrophoresis on an 8% polyacrylamide gel (8% acrylamide/N,N'-methylenebis(acrylamide) 29:1 [FUJIFILM Wako Pure Chemical Corporation, 015–25635], 0.15% v:v ammonium peroxodisulfate [FUJIFILM Wako Pure Chemical Corporation, 012–20503], and 0.05% v:v N,N,N',N'-tetramethylethylenediamine [FUJIFILM Wako Pure Chemical Corporation, 205–06313]) (for *Xbp1* detection) and 1% agarose gel (nacalai tesque, 01157–95) (for *Gapdh* detection) and visualized by ethidium bromide (FUJIFILM Wako Pure Chemical Corporation, 051–07811) staining and ChemiDoc XRS+ (BioRad, Hercules, CA) system. The expression levels of spliced

Xbp1 and *Gapdh* were quantified using Fiji software (ver. 2.0.0). *Gapdh* was used to normalize transcript levels. Quantitative PCR was performed on a Thermal Cycler Dice (Takara Bio, Shiga, Japan) using TB Green Premix Ex Taq II (Takara Bio, RR820B). mRNA levels were determined with the ΔΔCt method and normalized to *Actb* levels. The primer sequences are listed in **Table S3**.

TFEB nuclear translocation assay

PC12D cells were transfected with the pEGFP-N1-TFEB plasmid. At 48 h after the transfection, cells were selected with 0.8 mg/mL G418 (FUJIFILM Wako Pure Chemical Corporation, 071–06431) for 2 weeks. Cells stably expressing TFEB-GFP were treated with compounds for 1 h and then fixed with 3% paraformaldehyde containing 2 µg/mL Hoechst33342 for 30 min. Images were acquired using a confocal laser scanning microscope system (FV1000, Olympus, Tokyo, Japan). The percentage of TFEB nuclear translocation cells was quantified using Fiji software (ver. 2.0.0).

LysoTracker Red DND-99 staining

Differentiated PC12D cells seeded on a 35 mm glass-based dish (Iwaki, 11–0604-6) were stained with growth medium containing 50 nM LysoTracker Red DND-99 (Invitrogen, L7528) for 30 min. The cells were washed three times with LysoTracker-free growth medium and then immediately observed. Confocal microscopy was performed as above. Mean fluorescent intensity per cell in each image was quantified using Fiji software (ver. 2.0.0).

Aggresome staining

Aggresome staining was performed as previously described [45]. In brief, differentiated PC12D and SH-SY5Y cells seeded on coverslips were fixed with 3% paraformaldehyde, permeabilized with 0.3% Triton X-100 (FUJIFILM Wako Pure Chemical Corporation, 168–11805), 1% bovine serum albumin (Sigma-Aldrich, A8022) for 30 min, and blocked with 1% bovine serum albumin in 0.05% Tween-20 (FUJIFILM Wako Pure Chemical Corporation, 167–11515) in PBS (Cell Signaling Technology, 9808) for 60 min. Aggresomes were stained using the Proteostat Aggresome Detection Kit (Enzo Life Sciences, ENZ-51035-K100) according to the manufacturer's instructions. Samples were observed under confocal microscope as above, and quantitation was performed using Fiji software (ver. 2.0.0).

Clearance of mutant HTT

Differentiated PC12D cells were transfected with the pEGFP-Q23 or pEGFP-Q74 plasmid. At 48 h after the transfection, cells were treated with the indicated compounds for 24 h. Cells were then fixed with 3% paraformaldehyde and observed under confocal microscope as above. Percentage of cells with GFP-HTT aggregates to GFP-positive cells was calculated in each sample.

Primary neuronal cell culture and LDH assay

The primary cultured rat cortical neurons were collected from Wister rat embryos at embryonic day 18 and incubated with 0.03% papain in Hank's balanced salt solution (HBSS; Gibco, 14025076) for 5 min at 37°C. After dissociation with 10% FBS in neuronal culture medium (Neurobasal Plus medium [Gibco, A3582901] supplemented with 0.5 mM L-glutamine, penicillin-streptomycin, 2% B-27 supplement [Gibco, A3582801]), tissues were rinsed three times with HBSS, resuspended in neuronal culture medium, and filtered through a 70 µm nylon cell strainer to remove debris. The dissociated cells were plated onto poly-D-lysine-coated 96-well plates (Corning, 354640) at a density of 3×10^4 cells/well. After 48 h, half of the medium was replaced with fresh neuronal culture medium, and cells were treated with 16.7 µg/mL Uridine (Sigma-Aldrich, U3750) and 6.7 µg/mL 5-Fluoro-2′-deoxyuridine (Sigma-Aldrich, F0503) for 4 d to suppress the proliferation of non-neural cell types. Cells were then maintained with half of the medium replaced every 3 or 4 d. On day 14, cells were treated with various compounds for 24 h. After treatment, 100 µL of the cell culture medium was collected, and LDH levels released from damaged cells were measured using a Cytotoxicity LDH Assay Kit-WST (Dojindo, CK12) according to the manufacturer's instructions. The absorbance at 490 nm was measured by a plate reader (SpectraMax iD3, Molecular Devices, Tokyo, Japan). The study was approved by the Animal Experiment Committee (Approval No. 310261), and were performed in accordance with national, institutional and the ARRIVE guidelines.

Statistical analyses

All data are presented as the mean ± standard deviation (SD). Statistical analyses were performed with the two-tailed non-paired Student's t-test unless otherwise stated. All analyses were conducted using SPSS statistics software (ver. 24; IBM).

Disclosure statement

The authors declare no competing financial interests.

Funding

ORCID

Kazuo Shin-Ya 🔸 http://orcid.org/0000-0002-4702-0661
Masaya Imoto 🔸 http://orcid.org/0000-0003-4910-3871

References

[1] Klionsky DJ, Abdelmohsen K, Abe A, et al. Guidelines for the use and interpretation of assays for monitoring autophagy (3rd edition). Autophagy. 2016;12(1):1–222.

[2] Nixon RA. The role of autophagy in neurodegenerative disease. Nat Med. 2013 Aug;19(8):983–997.

[3] Sarkar S. Regulation of autophagy by mTOR-dependent and mTOR-independent pathways: autophagy dysfunction in neurodegenerative diseases and therapeutic application of autophagy enhancers. Biochem Soc Trans. 2013 Oct;41(5):1103–1130.

[4] Williams A, Sarkar S, Cuddon P, et al. Novel targets for Huntington's disease in an mTOR-independent autophagy pathway. Nat Chem Biol. 2008 May;4(5):295–305.

[5] Dunlop EA, Tee AR. mTOR and autophagy: a dynamic relationship governed by nutrients and energy. Semin Cell Dev Biol. 2014 Dec;36:121–129.

[6] Martina JA, Chen Y, Gucek M, et al. MTORC1 functions as a transcriptional regulator of autophagy by preventing nuclear transport of TFEB. Autophagy. 2012 Jun;8(6):903–914.

[7] Zhou J, Liao W, Yang J, et al. FOXO3 induces FOXO1-dependent autophagy by activating the AKT1 signaling pathway. Autophagy. 2012 Dec;8(12):1712–1723.

[8] Song S, Tan J, Miao Y, et al. Crosstalk of ER stress-mediated autophagy and ER-phagy: involvement of UPR and the core autophagy machinery. J Cell Physiol. 2018 May;233(5):3867–3874.

[9] Magi S, Tashiro E, Imoto M. A chemical genomic study identifying diversity in cell migration signaling in cancer cells. Sci Rep. 2012;2:823.

[10] Hirano K, Fujimaki M, Sasazawa Y, et al. Neuroprotective effects of memantine via enhancement of autophagy. Biochem Biophys Res Commun. 2019 Oct 8;518(1):161–170.

[11] Nicolau-Galmes F, Asumendi A, Alonso-Tejerina E, et al. Terfenadine induces apoptosis and autophagy in melanoma cells through ROS-dependent and -independent mechanisms. Apoptosis. 2011 Dec;16(12):1253–1267.

[12] Olzmann JA, Li L, Chin LS. Aggresome formation and neurodegenerative diseases: therapeutic implications. Curr Med Chem. 2008;15(1):47–60.

[13] Kaizuka T, Morishita H, Hama Y, et al. An autophagic flux probe that releases an internal control. Mol Cell. 2016 Nov 17;64(4):835–849.

[14] Xi H, Kurtoglu M, Liu H, et al. 2-Deoxy-D-glucose activates autophagy via endoplasmic reticulum stress rather than ATP depletion. Cancer Chemother Pharmacol. 2011 Apr;67(4):899–910.

[15] Kornicka K, Szlapka-Kosarzewska J, Smieszek A, et al. 5-Azacytydine and resveratrol reverse senescence and ageing of adipose stem cells via modulation of mitochondrial dynamics and autophagy. J Cell Mol Med. 2019 Jan;23(1):237–259.

[16] Selimovic D, Porzig BB, El-Khattouti A, et al. Bortezomib/proteasome inhibitor triggers both apoptosis and autophagy-dependent pathways in melanoma cells. Cell Signal. 2013 Jan;25(1):308–318.

[17] Ding WX, Ni HM, Gao W, et al. Differential effects of endoplasmic reticulum stress-induced autophagy on cell survival. J Biol Chem. 2007 Feb 16;282(7):4702–4710.

[18] Geng X, Ma L, Li Z, et al. Bromocriptine induces autophagy-dependent cell death in pituitary adenomas. World Neurosurg. 2017 Apr;100:407–416.

[19] You L, Shou J, Deng D, et al. Crizotinib induces autophagy through inhibition of the STAT3 pathway in multiple lung cancer cell lines. Oncotarget. 2015 Nov 24;6(37):40268–40282.

[20] Yoo YM, Jeung EB. Melatonin suppresses cyclosporine A-induced autophagy in rat pituitary GH3 cells. J Pineal Res. 2010 Apr;48(3):204–211.

[21] Milano V, Piao Y, LaFortune T, et al. Dasatinib-induced autophagy is enhanced in combination with temozolomide in glioma. Mol Cancer Ther. 2009 Feb;8(2):394–406.

[22] Wu Y, Li X, Xie W, et al. Neuroprotection of deferoxamine on rotenone-induced injury via accumulation of HIF-1 alpha and induction of autophagy in SH-SY5Y cells. Neurochem Int. 2010 Oct;57(3):198–205.

[23] Dou Q, Chen HN, Wang K, et al. Ivermectin induces cytostatic autophagy by blocking the PAK1/Akt axis in breast cancer. Cancer Res. 2016 Aug 1;76(15):4457–4469.

[24] Sarkar S, Floto RA, Berger Z, et al. Lithium induces autophagy by inhibiting inositol monophosphatase. J Cell Biol. 2005 Sep 26;170(7):1101–1111.

[25] Bao W, Gu Y, Ta L, et al. Induction of autophagy by the MG132 proteasome inhibitor is associated with endoplasmic reticulum stress in MCF7 cells. Mol Med Rep. 2016 Jan;13(1):796–804.

[26] Jung CH, Ro SH, Cao J, et al. mTOR regulation of autophagy. FEBS Lett. 2010 Apr 2;584(7):1287–1295.

[27] Morselli E, Marino G, Bennetzen MV, et al. Spermidine and resveratrol induce autophagy by distinct pathways converging on the acetylproteome. J Cell Biol. 2011 Feb 21;192(4):615–629.

[28] Oh M, Choi IK, Kwon HJ. Inhibition of histone deacetylase1 induces autophagy. Biochem Biophys Res Commun. 2008 May 16;369(4):1179–1183.

[29] Prieto-Dominguez N, Ordonez R, Fernandez A, et al. Modulation of Autophagy by Sorafenib: effects on Treatment Response. Front Pharmacol. 2016;7:151.

[30] Ha JY, Kim JS, Kim SE, et al. Simultaneous activation of mitophagy and autophagy by staurosporine protects against dopaminergic neuronal cell death. Neurosci Lett. 2014 Feb;21(561):101–106.

[31] Thoreen CC, Kang SA, Chang JW, et al. An ATP-competitive mammalian target of rapamycin inhibitor reveals rapamycin-resistant functions of mTORC1. J Biol Chem. 2009 Mar 20;284(12):8023–8032.

[32] Zhang J, Ng S, Wang J, et al. Histone deacetylase inhibitors induce autophagy through FOXO1-dependent pathways. Autophagy. 2015 Apr 3;11(4):629–642.

[33] Sakamaki JI, Wilkinson S, Hahn M, et al. Bromodomain protein BRD4 is a transcriptional repressor of autophagy and lysosomal function. Mol Cell. 2017 May 18;66(4):517–532.e9.

[34] Wu Q, Wang X, Nepovimova E, et al. Mechanism of cyclosporine A nephrotoxicity: oxidative stress, autophagy, and signalings. Food Chem Toxicol. 2018 Aug;118:889–907.

[35] Atkins C, Liu Q, Minthorn E, et al. Characterization of a novel PERK kinase inhibitor with antitumor and antiangiogenic activity. Cancer Res. 2013 Mar 15;73(6):1993–2002.

[36] Bertolotti A, Zhang Y, Hendershot LM, et al. Dynamic interaction of BiP and ER stress transducers in the unfolded-protein response. Nat Cell Biol. 2000 Jun;2(6):326–332.

[37] Harding HP, Zhang Y, Ron D. Protein translation and folding are coupled by an endoplasmic-reticulum-resident kinase. Nature. 1999 Jan 21;397(6716):271–274.

[38] Pakos-Zebrucka K, Koryga I, Mnich K, et al. The integrated stress response. EMBO Rep. 2016 Oct;17(10):1374–1395.

[39] Kimura S, Noda T, Yoshimori T. Dissection of the autophagosome maturation process by a novel reporter protein, tandem fluorescent-tagged LC3. Autophagy. 2007 Sep-Oct;3(5):452–460.

[40] Kiga M, Tanzawa F, Iwasaki S, et al. Antitumor effects of novel highly hydrophilic and non-ATP-competitive MEK1/2 inhibitor, SMK-17. Anticancer Drugs. 2012 Jan;23(1):119–130.

[41] Settembre C, Di MC, VA P, et al. TFEB links autophagy to lysosomal biogenesis. Science. 2011 Jun 17;332(6036):1429–1433.

[42] Settembre C, Zoncu R, Medina DL, et al. A lysosome-to-nucleus signalling mechanism senses and regulates the lysosome via mTOR and TFEB. Embo J. 2012 Mar 7;31(5):1095–1108.

[43] Rusmini P, Cortese K, Crippa V, et al. Trehalose induces autophagy via lysosomal-mediated TFEB activation in models of motoneuron degeneration. Autophagy. 2019 Apr;15(4):631–651.

[44] Li Y, Xu M, Ding X, et al. Protein kinase C controls lysosome biogenesis independently of mTORC1. Nat Cell Biol. 2016 Oct;18 (10):1065–1077.

[45] Kataura T, Saiki S, Ishikawa KI, et al. BRUP-1, an intracellular bilirubin modulator, exerts neuroprotective activity in a cellular Parkinson's disease model. J Neurochem. 2020 Mar 3. DOI:10.1111/jnc.14997.

[46] Lin MT, Beal MF. Mitochondrial dysfunction and oxidative stress in neurodegenerative diseases. Nature. 2006 Oct 19;443(7113):787–795.

[47] Shinjo S, Mizotani Y, Tashiro E, et al. Comparative analysis of the expression patterns of UPR-target genes caused by UPR-inducing compounds. Biosci Biotechnol Biochem. 2013;77(4):729–735.

[48] Reisberg B, Doody R, Stoffler A, et al. Memantine in moderate-to-severe Alzheimer's disease. N Engl J Med. 2003 Apr 3;348(14):1333–1341.

[49] Verhagen Metman L, Del Dotto P, van den Munckhof P, et al. Amantadine as treatment for dyskinesias and motor fluctuations in Parkinson's disease. Neurology. 1998 May;50(5):1323–1326.

[50] Johnson JW, Kotermanski SE. Mechanism of action of memantine. Curr Opin Pharmacol. 2006 Feb;6(1):61–67.

[51] Hayashi T. The Sigma-1 receptor in cellular stress signaling. Front Neurosci. 2019;13:733.

[52] Kubickova J, Lencesova L, Csaderova L, et al. Haloperidol affects plasticity of differentiated NG-108 cells through sigma1R/IP3R1 complex. Cell Mol Neurobiol. 2018 Jan;38(1):181–194.

[53] Nishitoh H, Matsuzawa A, Tobiume K, et al. ASK1 is essential for endoplasmic reticulum stress-induced neuronal cell death triggered by expanded polyglutamine repeats. Genes Dev. 2002 Jun 1;16(11):1345–1355.

[54] Ogata M, Hino S, Saito A, et al. Autophagy is activated for cell survival after endoplasmic reticulum stress. Mol Cell Biol. 2006 Dec;26(24):9220–9231.

[55] Margariti A, Li H, Chen T, et al. XBP1 mRNA splicing triggers an autophagic response in endothelial cells through BECLIN-1 transcriptional activation. J Biol Chem. 2013 Jan 11;288(2):859–872.

[56] Green AJ, Gelfand JM, Cree BA, et al. Clemastine fumarate as a remyelinating therapy for multiple sclerosis (ReBUILD): a randomised, controlled, double-blind, crossover trial. Lancet. 2017 Dec 2;390(10111):2481–2489.

[57] Apolloni S, Fabbrizio P, Parisi C, et al. Clemastine confers neuroprotection and induces an anti-inflammatory phenotype in SOD1(G93A) mouse model of amyotrophic lateral sclerosis. Mol Neurobiol. 2016 Jan;53(1):518–531.

[58] Apolloni S, Fabbrizio P, Amadio S, et al. Actions of the antihistaminergic clemastine on presymptomatic SOD1-G93A mice ameliorate ALS disease progression. J Neuroinflammation. 2016 Aug 22;13(1):191.

[59] Hu WW, Yang Y, Wang Z, et al. H1-antihistamines induce vacuolation in astrocytes through macroautophagy. Toxicol Appl Pharmacol. 2012 Apr 15;260(2):115–123.

[60] Jakhar R, Paul S, Bhardwaj M, et al. Astemizole-Histamine induces Beclin-1-independent autophagy by targeting p53-dependent crosstalk between autophagy and apoptosis. Cancer Lett. 2016 Mar 1;372(1):89–100.

[61] Jangi SM, Ruiz-Larrea MB, Nicolau-Galmes F, et al. Terfenadine-induced apoptosis in human melanoma cells is mediated through Ca2+ homeostasis modulation and tyrosine kinase activity, independently of H1 histamine receptors. Carcinogenesis. 2008 Mar;29(3):500–509.

[62] Zheng ZY, Li J, Li F, et al. Induction of N-Ras degradation by flunarizine-mediated autophagy. Sci Rep. 2018 Nov 16;8(1):16932.

[63] B'Chir W, Maurin AC, Carraro V, et al. The eIF2alpha/ATF4 pathway is essential for stress-induced autophagy gene expression. Nucleic Acids Res. 2013 Sep;41(16):7683–7699.

[64] Py BF, Boyce M, Yuan J. A critical role of eEF-2K in mediating autophagy in response to multiple cellular stresses. Autophagy. 2009 Apr;5(3):393–396.

[65] Dever TE. Gene-specific regulation by general translation factors. Cell. 2002 Feb 22;108(4):545–556.

[66] Kiga M, Nakayama A, Shikata Y, et al. SMK-17, a MEK1/2--specific inhibitor, selectively induces apoptosis in beta-catenin-mutated tumors. Sci Rep. 2015 Feb 2;5(1):8155.

[67] Kinsey CG, Camolotto SA, Boespflug AM, et al. Protective autophagy elicited by RAF–>MEK–>ERK inhibition suggests a treatment strategy for RAS-driven cancers. Nat Med. 2019 Apr;25(4):620–627.

[68] Chauhan S, Goodwin JG, Chauhan S, et al. ZKSCAN3 is a master transcriptional repressor of autophagy. Mol Cell. 2013 Apr 11;50 (1):16–28.

[69] Le Good JA, Ziegler WH, Parekh DB, et al. Protein kinase C isotypes controlled by phosphoinositide 3-kinase through the protein kinase PDK1. Science. 1998 Sep 25;281(5385): 2042–2045.

[70] Saiki S, Sato S, Hattori N. Molecular pathogenesis of Parkinson's disease: update. J Neurol Neurosurg Psychiatry. 2012 Apr;83 (4):430–436.

[71] Squier TC. Oxidative stress and protein aggregation during biological aging. Exp Gerontol. 2001 Sep;36(9):1539–1550.

[72] Kao C, Chao A, Tsai CL, et al. Bortezomib enhances cancer cell death by blocking the autophagic flux through stimulating ERK phosphorylation. Cell Death Dis. 2014 Nov;6(5):e1510.

[73] Ji MM, Lee JM, Mon H, et al. Proteasome inhibitor MG132 impairs autophagic flux through compromising formation of autophagosomes in Bombyx cells. Biochem Biophys Res Commun. 2016 Oct 28;479(4):690–696.

[74] Wang D, Xu Q, Yuan Q, et al. Proteasome inhibition boosts autophagic degradation of ubiquitinated-AGR2 and enhances the antitumor efficiency of bevacizumab. Oncogene. 2019 May;38(18):3458–3474.

[75] Glickman MH, Ciechanover A. The ubiquitin-proteasome proteolytic pathway: destruction for the sake of construction. Physiol Rev. 2002 Apr;82(2):373–428.

[76] Marambio P, Toro B, Sanhueza C, et al. Glucose deprivation causes oxidative stress and stimulates aggresome formation and autophagy in cultured cardiac myocytes. Biochim Biophys Acta. 2010 Jun;1802(6):509–518.

[77] Katoh-Semba R, Kitajima S, Yamazaki Y, et al. Neuritic growth from a new subline of PC12 pheochromocytoma cells: cyclic AMP mimics the action of nerve growth factor. J Neurosci Res. 1987;17 (1):36–44.

[78] Suzuki A, Obi K, Urabe T, et al. Feasibility of ex vivo gene therapy for neurological disorders using the new retroviral vector GCDNsap packaged in the vesicular stomatitis virus G protein. J Neurochem. 2002 Aug;82(4):953–960.

[79] Ory DS, Neugeboren BA, Mulligan RC. A stable human-derived packaging cell line for production of high titer retrovirus/vesicular stomatitis virus G pseudotypes. Proc Natl Acad Sci USA. 1996 Oct 15;93(21):11400–11406.

[80] Igarashi Y, Matsuoka N, In Y, et al. Nonthmicin, a polyether polyketide bearing a halogen-modified tetronate with neuroprotective and antiinvasive activity from actinomadura sp. Org Lett. 2017 Mar 17;19(6):1406–1409.

[81] Shikata Y, Yoshimaru T, Komatsu M, et al. Protein kinase A inhibition facilitates the antitumor activity of xanthohumol, a valosin-containing protein inhibitor. Cancer Sci. 2017 Apr;108 (4):785–794.